Cerebral Cortex, 2018; 1–23

doi: 10.1093/cercor/bhy124
Original Article

ORIGINAL ARTICLE

Human Pregenual Anterior Cingulate Cortex: Structural, Functional, and Connectional Heterogeneity

Nicola Palomero-Gallagher[1,2], Felix Hoffstaedter[3,4], Hartmut Mohlberg[1], Simon B. Eickhoff[3,4], Katrin Amunts[1,5,6] and Karl Zilles[1,2,6]

[1]Institute of Neuroscience and Medicine (INM-1), Research Centre Jülich, 52425 Jülich, Germany, [2]Department of Psychiatry, Psychotherapy and Psychosomatics, Medical Faculty, RWTH Aachen, 52074 Aachen, Germany, [3]Institute of Systems Neuroscience, Medical Faculty, Heinrich Heine University Düsseldorf 40225, Düsseldorf, Germany, [4]Institute of Neuroscience and Medicine (INM-7), Research Centre Jülich, 52425 Jülich, Germany, [5]C. & O. Vogt Institute for Brain Research, Heinrich-Heine-University, 40225 Düsseldorf, Germany and [6]JARA-BRAIN, Jülich-Aachen Research Alliance, 52425 Jülich, Germany

Address correspondence to Nicola Palomero-Gallagher, Institute of Neuroscience and Medicine (INM-1), Research Centre Jülich, 52425 Jülich, Germany. Email: n.palomero-gallagher@fz-juelich.de

Abstract

The human pregenual anterior cingulate cortex (pACC) encompasses 7 distinct cyto- and receptorarchitectonic areas. We lack a detailed understanding of the functions in which they are involved, and stereotaxic maps are not available. We present an integrated structural/functional map of pACC based on probabilistic cytoarchitectonic mapping and meta-analytic connectivity modeling and quantitative functional decoding. Due to the restricted spatial resolution of functional imaging data relative to the microstructural parcellation, areas p24a of the callosal sulcus and p24b on the surface of the cingulate gyrus were merged into a "gyral component" (p24ab) of area p24, and areas pv24c, pd24cv, and pd24cd, located within the cingulate sulcus were merged into a "sulcal component" (p24c) for meta-analytic analysis. Area p24ab was specifically associated with interoception, p24c with the inhibition of action, and p32, which was also activated by emotion induction tasks pertaining negatively valenced stimuli, with the ability to experience empathy. Thus, area p32 could be classified as cingulate association cortex playing a crucial role in the cognitive regulation of emotion. By this spectrum of functions, pACC is a structurally and functionally heterogeneous region, clearly differing from other parts of the anterior and middle cingulate cortex.

Key words: anterior cingulate cortex, cytoarchitecture, functional decoding, functional meta-analysis, human brain, probability maps

Introduction

The anterior cingulate cortex (ACC) occupies the rostral portion of Brodmann's (1909) *Subregio praecingularis* (which encompasses his areas 24, 25, 32, and 33), and is activated by diverse tasks ranging from emotion processing and regulation to attention and cognitive control (Bush et al. 2000; Allman et al. 2001; Paus 2001; Phan et al. 2002; Fellows and Farah 2005). The diversity of functional domains assigned to the ACC led to its segregation into pregenual (pACC) and subgenual (sACC) parts. Whereas sACC has been associated with the processing of negatively valenced

© The Author(s) 2019. Published by Oxford University Press.
This is an Open Access article distributed under the terms of the Creative Commons Attribution Non-Commercial License (http://creativecommons.org/licenses/by-nc/4.0/), which permits non-commercial re-use, distribution, and reproduction in any medium, provided the original work is properly cited. For commercial re-use, please contact journals.permissions@oup.com

stimuli and emotions (George et al. 1995; Phan et al. 2002; Kross et al. 2009; Smith et al. 2011; Palomero-Gallagher et al. 2015), pACC is thought to subserve the processing of positively valenced stimuli (Vogt et al. 2003). It is also activated by attention and conflict-monitoring tasks (Allman et al. 2001; Fellows and Farah 2005). This functional heterogeneity of the ACC is associated with regional variations in the functional connectivity profiles of the pregenual and subgenual portions of the cingulate gyrus, as repeatedly demonstrated by meta-analytic connectivity modeling studies (Beckmann et al. 2009; Torta and Cauda 2011; Torta et al. 2013).

The functionally driven subdivision of the ACC region is not reflected in the cytoarchitectonic maps of Brodmann (1909; Fig. 1A), Öngür et al. (2003), Petrides et al. (2012), or Vogt et al. (1995), where the ACC consists of semicircular fields which surround the corpus callosum, but without a separation into dorsal and ventral parts. However, a recent cytoarchitectonic study using quantitative analysis of cell-body distributions has demonstrated a higher structural differentiation of the ACC, which is further supported by a concomitant analysis of the regional and laminar distribution patterns of 15 different transmitter receptors (Palomero-Gallagher et al. 2008; Fig. 1B). This multimodal approach resulted in the definition of 12 areas within ACC, with 2 streams of structural differentiation: 1) 7 areas could be identified based on differences in the degree of laminar differentiation when moving from the corpus callosum towards the convexity of the hemisphere, 2) differences in the size and packing density layer III and layer V neurons within areas 24a, 24b, and 32, as well as the presence of area 25 ventral to the corpus callosum, enabled the definition of pregenual (encompassing areas p24a, p24b, pv24c, pd24cv, pd24cd, p32) and subgenual (encompassing areas s24a, s24b, pv24cd s32, 25) regions within the ACC (Palomero-Gallagher et al. 2008).

Areas of the sACC were recently brought into stereotaxic space, and the resulting volumes were used for a cytoarchitectonically informed quantitative meta-analysis which confirmed the significant association of sACC with the processing of negative emotions (Palomero-Gallagher et al. 2015). More specifically, distinct architectonic areas within sACC are associated with different kinds of negatively valenced emotional stimuli: s24 is activated during the processing of sadness, whereas s32 is activated during the processing of fear (Palomero-Gallagher et al. 2015). Furthermore, the probabilistic maps of sACC areas highlight the lack of a correspondence between macroscopic landmarks and the borders of all areas except for those of area 33, which was always buried in the callosal sulcus.

Comparable information, however, is not currently available for pACC areas. Therefore, the current study aims to present an integrated structural/functional map of pACC based on cytoarchitectonic mapping resulting in probabilistic, stereotaxic maps in combination with a meta-analysis of functional imaging data. The results of the present study demonstrate a remarkable involvement of this brain region in the processing of negatively valenced stimuli, though not in that of happiness. In addition to its role in emotion induction, pACC contributes considerably to cognitive functions such as social cognition, including theory of mind tasks, and conflict-monitoring.

Material and Methods

Continuous Probabilistic Maps and Maximum Probability Maps

We examined the cytoarchiteture of pACC areas in 10 *postmortem* fixed human brains (Table 1) scanned with a T1-weighted magnetic resonance sequence ("MR volume"; flip angle = 40°; repetition time TR = 40 ms; echo time TE = 5 ms for each image; 128 sagittal sections; spatial resolution 1 × 1 × 1.17 mm; 8 bit gray value resolution) before histological processing. Brains were embedded in paraffin and serially sectioned (20 µm thick sections) in the coronal (6 cases) or horizontal (4 cases) plane with a large-scale microtome. Each 15th section was mounted on gelatine-coated slides, stained for cell bodies with a modified silver cell-body staining (Merker 1983; Palomero-Gallagher et al. 2008), and digitized in a flatbed scanner (Epson Perfection V750 Pro; 1200 dpi, 20 µm per pixel).

Areas p24a, p24b, pv24c, pd24cv, pd24cd, and p32 had been previously identified by an observer-independent cytoarchitectonic mapping approach (Fig. 1B), and their existence was confirmed by an additional multi-receptor analysis (Zilles et al. 2002; Schleicher et al. 2005; Palomero-Gallagher et al. 2008). However, in our previous study (Palomero-Gallagher et al.

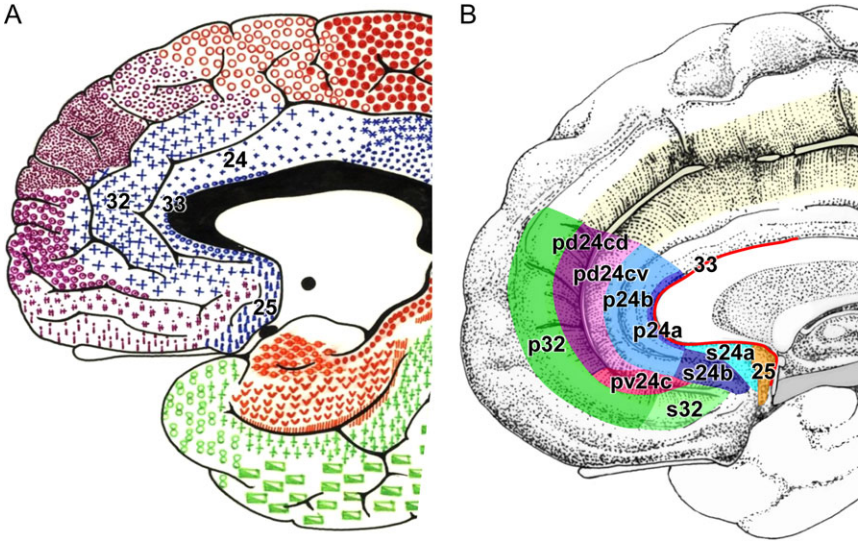

Figure 1. Parcellations of the cingulate cortex by (*A*) Brodmann (1910) and (*B*) Palomero-Gallagher et al. (2008). Note that the anterior cingulate cortex only covers the rostral portion of Brodmann's Subregio praecingularis (which encompasses his areas 24, 25, 32, and 33).

Table 1 Brains used for the computation of probabilistic maps of pACC areas.

Brain ID	Gender	Age	Fresh weight (g)	Cause of death	Plane of sectioning
1	Female	79	1350	Carcinoma of the bladder	Coronal
5	Female	59	1142	Cardiorespiratory insufficiency	Coronal
6	Male	54	1757	Myocardial infarction	Coronal
7	Male	37	1437	Cardiac arrest	Coronal
10	Female	85	1046	Mesenteric artery infarction	Coronal
11	Male	74	1381	Myocardial infarction	Coronal
15	Male	54	1248	Bullet wound	Horizontal
16	Male	63	1393	Accident, internal bleeding	Horizontal
17	Female	50	1328	Myocardial infarction	Horizontal
18	Female	75	1310	Cardiac arrest	Horizontal

Cytoarchitectonic criteria used for the definition of these areas published in Palomero-Gallagher et al. (2008). Brain identification number is according to designations of the brain bank from which the brains were collected.

2008), we only described the cyto- and receptorarchitectonic features characterizing each of the identified areas, but provided no information concerning the intersubject variability in their size and location, or of the relationship between borders between areas and macroscopical landmarks. These aspects, together with a characterization of the functional and connectivity profiles of pACC areas are the subject of the present study.

In the present study, we merged specific cyto- and receptorarchitectonically identified areas for computation of probabilistic maps. This decision was driven by 3 main reasons: 1) The restricted spatial resolution of functional imaging data relative to the microstructural parcellation and the high degree of structural segregation found within the pACC, 2) the necessity to integrate different spatial and temporal scales and data modalities into a common reference system to create interoperable multimodal human brain models (Amunts et al. 2014), and 3) the differential connectivity patterns of the gyral and sulcal portions of the cingulate cortex (Vogt and Pandya 1987; Morecraft et al. 2012). Consequently, areas p24a of the callosal sulcus and p24b on the surface of the cingulate gyrus were merged into a "gyral component" (p24ab) of area p24. Areas pv24c, pd24cv, and pd24cd located within the cingulate sulcus were merged into a "sulcal component" (p24c) of area p24. Thus, although the extent of all architectonically identified pACC areas was interactively traced in the high-resolution images of the histological sections using in-house software (SectionTracer), traces were used for the 3D-reconstruction of only of merged areas p24ab and p24c, as well as of p32. The SectionTracer software (programmed in Java) produces asci files with the coordinates of nodes in the traces of each area relative to the top left corner of the high-resolution image of the histological section containing the area in question, and which are used for the subsequent 3D-reconstruction steps in the pipeline.

The histological volume of each brain was 3D-reconstructed by linear and non-linear registrations to its MR volume (Hömke 2006) to enable correction of deformations and shrinkage inevitably caused by histological techniques. Prior to this step, images of the entire brains were separated by means of labeled masks into left and right hemispheres, and those images of the separated hemispheres were iteratively corrected using a section-by-section elastic alignment of adjacent sections at high-resolution (Mohlberg et al. 2012). Finally, the ensuing histological volumes were spatially normalized to the corresponding hemispheres of the single-subject T1-weighted MNI reference brain (Evans et al. 2012) in anatomical MNI space (Amunts et al. 2005) with an affine and non-linear elastic registration approach (Henn et al. 1997; Hömke 2006). Cytoarchitectonic areas delineated in the 10 individual *postmortem* brains could thus be registered to the stereotaxic reference template brain. Having all brains and delineations in the same reference space enabled computation of continuous probabilistic maps for each pACC area in anatomical MNI space. The probabilistic map of a given area encodes for each voxel of the reference brain how many individual brains showed the respective cytoarchitectonic area in that voxel. Thus, continuous probability maps quantitatively describe the intersubject variability of a cortical area in stereotaxic space. Maximum probability maps (MPMs) were then calculated by assigning each voxel of the reference brain to the cytoarchitectonic area with the highest probability in that voxel (Eickhoff et al. 2005, 2006). If 2 areas shared the same probability in a particular voxel, this voxel was assigned to the area with the higher average probabilities in directly adjacent voxels (Eickhoff et al. 2005, 2006). A threshold of 40% was applied to those voxels where the delineated pACC area abutted cortical regions which have not yet been mapped using the observer-independent cytoarchitectonic approach (i.e., BA8 or BA9 at the dorsal border of area p32).

These probabilistic maps quantitatively express the intersubject variability of a cortical area in stereotaxic space. They can be viewed as surface representations through the JuBrain atlas (http://www.jubrain.fz-juelich.de/apps/cytoviewer/cytoviewer-main.php), or downloaded at www.fz-juelich.de/inm/inm-1/spm_anatomy_toolbox for the analysis of functional or structural magnetic resonance imaging data by means of the Anatomy Toolbox (Eickhoff et al. 2005).

Volumetry

The traces of p24ab, p24c, and p32 on the digital images of the histological sections were used to calculate the volumes (V, in mm^3) of each area using Cavalieri's principle (Amunts et al. 2005) according to:

$$V = s \cdot \Delta x \cdot \Delta y \cdot F \cdot \Sigma N_i$$

where the distance (s) between 2 measured sections was 1.2 mm, pixel size (Δx and Δy) was 0.02116 × 0.02116 mm, F was the individual shrinkage factor of each brain caused by the histological processing, and N_i the number of pixels of the cortical area in section i. The individual shrinkage factor was calculated for each

brain as the ratio between the fresh volume of the brain and its volume after histological processing (Amunts et al. 2005).

Volumes of pACC areas were further analyzed with respect to interhemispheric and gender differences, as well as for the interaction between gender and hemisphere using Monte-Carlo permutation tests (Palomero-Gallagher et al. 2015), and *P*-values were Bonferroni corrected for multiple testing. In order to compensate the trend of male brains to larger volumes compared to female brains (Luders et al. 2014; Perlaki et al. 2014), all areal volumes were expressed as a fraction of total brain volume for each brain prior to statistical analysis. Gender differences were analyzed by first computing difference in the mean volumes between the 5 male and 5 female brains, then randomly reassigning each brain to one of the 2 groups (male/female), and re-computing the respective difference between the mean volumes of the ensuing randomly assembled groups was calculated. This difference obtained under the null-hypothesis of label exchangeability (i.e., that brain assignment to a gender group is irrelevant) was recorded, and the procedure repeated 10^6 times. The true gender difference was considered significant if it was larger than 95% of the values under the empirical null-distribution ($P < 0.05$; Bonferroni corrected for multiple comparisons). Interhemispheric differences were analyzed by means of a within-subject design. We first determined the average interhemispheric difference for the ensuing paired-test design by computing the differences between left and right areal volumes in each brain. We then randomly and independently across subjects designated the 2 measurements as "left" or "right", and the mean differences between "left" and "right" areal volumes across subjects were calculated, providing a difference value for each area under the null-hypothesis that left and right values were not systematically different. This procedure was repeated 10^6 times and interhemispheric differences were considered significant if they were larger than 95% of the values under the empirical null-distribution ($P < 0.05$; Bonferroni corrected for multiple comparisons).

Connectivity and Function of the sACC Areas

We examined task-based functional connectivity and functional associations of cytoarchitectonically defined areas p24ab, p24c, and p32 using meta-analytic connectivity modeling (MACM; Eickhoff et al. 2010; Langner et al. 2014) and quantitative functional decoding (Cieslik et al. 2013; Rottschy et al. 2013), respectively, based on the BrainMap database (www.brainmap.org; Fox and Lancaster 2002; Fox et al. 2014). The MPM representation of each area was used to define the volumes of interest. The BrainMap database contained over 15 000 neuroimaging experiments at the time of analysis, and we considered all stereotaxic coordinates from mapping studies without interventions or group comparisons (amounting to approximately 7500 studies) in healthy subjects using either fMRI or PET, because a preselection of taxonomic categories would result in a fairly strong a priori hypothesis about how brain networks are organized.

The MACM analysis determines the convergence of foci reported in different experiments that also activate the delineated regions, and these co-activation foci were modeled as probability distributions based on the spatial uncertainty due to the between-subject and between-template variability of neuroimaging data. Co-activation patterns were assessed using the activation likelihood estimation (ALE) non-parametric statistical approach (Eickhoff et al. 2012). To identify non-random clusters of convergence over studies, the obtained ALE values were compared with a null-distribution reflecting a random spatial association between the considered experiments. The analysis was thresholded at a cluster-level FWE corrected $P < 0.05$ (cluster-forming threshold at voxel-level $P < 0.001$), which provides optimal balance between sensitivity and specificity as shown in a large-scale simulation (Eickhoff, Nichols et al. 2016). Pairwise conjunctions over all areas were also computed to determine possible similarities in the co-activation patterns of pACC areas. Additionally, voxel-wise differences of the ALE scores from the individual MACM analyses were computed to assess differential co-activation between areas, and thresholded at a posterior probability of $P < 0.95$ for a true difference using permutation testing ($n = 5000$; Eickhoff et al. 2018). The resulting difference maps were masked with the main effect of the respective cytoarchitectonic pACC area. Only clusters including at least 50 voxels are reported.

Functional characterization of pACC areas was based on filtering the BrainMap database for experiments activating the respective MPMs followed by forward and reverse inference analyses (cf. Cieslik et al. 2013; Rottschy et al. 2013) of the functional descriptions (i.e., the meta-data "Behavioural Domains" and "Paradigm Classes") of the experiments that activate a particular area. The Behavioural Domains in BrainMap classify mental operations isolated by the experiments into 6 main categories (action, cognition, emotion, interoception, perception, and pharmacology), whereas the Paradigm Classes represent the specific experimental task used in the respective experiment (Fox, Laird et al. 2005). In the forward inference, the functional profile was determined by identifying those taxonomic labels for which the probability of finding activation in the region of interest was significantly higher than the overall chance across the entire database of finding activation in that particular region. We identified significant associations by means of a binomial test ($P < 0.05$, corrected for multiple comparisons using false discovery rate) to determine whether the conditional probability of activation for a specific label [P(Activation|Task)] was higher than the baseline probability of activating the region(s) in question per se [P(Activation)]. In the reverse inference [P(Task|Activation)], the functional profile was determined by identifying the most probable behavioral domains and Paradigm Classes given activation in a specific region, and was derived from P(Activation|Task) as well as P(Task) and P(Activation) using Bayes' rule. Significance (at $P < 0.05$, corrected for multiple comparisons using false discovery rate) was assessed by means of a chi-squared test. Specifically, for each Behavioural Domain and Paradigm Class category, the number of activation foci associated with this meta-data category was assessed within a seed volume (an MPM of a given pACC area), and compared against the number of foci which would be expected for this category given the entire database. The expected number of foci for a category was determined by multiplying the total number of foci for the current category with the proportion of foci in BrainMap located within the respective seed volume.

Results

Relationship Between Areal Borders and Macroscopic Landmarks

Macroscopic landmarks provide an orientation point for some of the borders within the pACC region, though only when moving from the corpus callosum to the superior margin of the hemisphere, as described in the following paragraphs. Although the

callosal sulcus is a reliable marker for the caudal most portion of pACC, no macroscopic landmarks could be associated with the remaining "outer" borders of this region. Thus the boundaries of pACC areas with ventrally adjacent areas of the sACC region, with the rostrally/dorsally located frontal and medial prefrontal areas, or with the caudally following midcingulate areas can only be identified by cytoarchitectonic analysis (Fig. 2).

The lateral border of p24a, where it abuts area 33, was always located within the callosal sulcus. The degree to which p24a encroached onto the surface of the cingulate gyrus, where it abuts p24b, varied depending on the depth of the callosal sulcus. Area p24a reached its greatest extent on the gyral surface when the callosal sulcus was particularly shallow. The lateral border of p24b was found mainly within the cingulate sulcus, though very close to the surface, where it abutted area pv24c ventrally and pd24cv dorsally. Areas p24a and p24b were merged into a "gyral component of area p24", i.e., area p24ab for volumetric analysis and computation of continuous probability maps. Given the extent of areas p24a and p24b, area p24ab always occupied the free surface of the cingulate gyrus and encroached into the callosal and cingulate sulci.

Areas pv24c, pd24cv, and pd24cd were mostly buried within the cingulate sulcus. Only when the sulcus was interrupted or became extremely shallow, as was the case in the left hemispheres of cases 10, 11, and 17 (Fig. 2), did pd24cv reach the gyral surface (Fig. 3). The border between pd24cv and pd24cd was located in, or very close to, the fundus of the cingulate sulcus. No macroscopic landmark marked the transition from pv24c to pd24cv. Areas pv24c, pd24cv and pd24cd were merged into a "sulcal component of area p24", i.e., area p24c for volumetric analysis and computation of continuous probability maps, and this area p24c was always located within the cingulate sulcus.

The border between areas p32 and p24c was located in the cingulate sulcus, and always within the outer third of the sulcal wall. The border between p32 and orbitofrontal cortical areas was found either on the gyral surface, of within the superior rostral or paracingulate sulci, depending on their length and course, and on whether they merged or not. Likewise, the border between p32 and adjacent frontopolar and medial prefrontal areas could be found either on a gyral surface, or within the paracingulate sulcus, depending on both variability pertaining the extent of the area and whether the sulcus was interrupted or continuous. The paracingulate sulcus was present in all 20 hemispheres, but was continuous only in 5 (namely in the left one of brains #1, #6, #10, #17 and #18), and fragmented in the right hemisphere of cases #10 and #15 (Fig. 2). Additionally, the paracingulate and superior rostral sulci only merged in 6 left (cases #1, #5, #6, #15, #17, and #18) and 6 right (cases #1, #6, #10, #15, #17, and #18) hemispheres. Even when present, the paracingulate sulcus was not a consistent marker of the border, because at times area p32 extended further rostrally, as seen in the right hemispheres of case #1 and #6, where p32 was clearly visible on the surface of the inferior rostral and superior frontal gyri, respectively (Fig. 2). Conversely, in both hemispheres of case #5 the ventral portion of area p32 is restricted to the superior cingulate gyrus, and did not even encroach into the paracingulate sulcus (Figure 2). Finally, the position of the border within the paracingulate sulcus was not constant, and was found on either of its banks or close to the fundus, depending on the hemisphere examined. Therefore, we can state that no reliable macroscopic landmark could be consistently associated with the outer borders of p32.

Volumetric Analysis

Area p32 was the largest of the pACC areas, reaching 3467 mm^3 in the right hemisphere of male brains, whereas p24ab and p24c were comparable in size (Table 2). Statistical analysis of the histological volumes corrected for individual brain sizes revealed no interhemispheric or gender differences, or interactions between gender and hemisphere in any of the examined areas.

Probabilistic Maps and Variability

Areas p24ab, p24c, and p32 were registered to the MNI reference brain in order to compute continuous probability maps and quantify intersubject variability of their size and location (Fig. 4A–C). p32 was the least variable area, since it presented the largest number of voxels with the highest overlap of all 10 brains, and p24c was the area with the highest intersubject variability.

Since continuous probability maps of different adjoining areas overlap, we computed MPMs, which present a contiguous, non-overlapping parcellation of the pACC. These MPMs reflect, for each voxel, the most likely area at that position in a sample of 10 human *postmortem* brains (Fig. 4D).

Task-Dependent Functional Connectivity

Task-based co-activations of p24ab, p24c, and p32 were quantitatively mapped using the BrainMap database. We found 231 experiments in the BrainMap database which described activation foci in p24ab (a full list of the articles is provided in Supplementary reference list 1). It comprises a total of 3848 subjects and 3011 foci (see Supplementary Fig. 1A). A total of 197 experiments (encompassing 3030 subjects and 2636 foci, Supplementary Fig. 1B) reported activations in p24c (Supplementary reference list 2). Area p32 was reported to be activated in 585 experiments encompassing 8590 subjects and 6832 foci (Supplementary Fig. 1C; Supplementary reference list 3). Meta-analytic connectivity modeling of these data revealed distinct patterns of co-activation clusters for each of the pACC areas.

p24ab presented the most restricted co-activation pattern, with only 3 co-activated clusters, which included both cortical and subcortical structures (Fig. 5A, Table 3). Bilateral maxima were located in the anterior insula, ventral posterior cingulate cortex (vPCC), ventral striatum, and in the portion of the mediodorsal thalamic nucleus connected with the prefrontal cortex (MDpr). Lateralized co-activation clusters presented maxima in the right middle frontal gyrus (dorsal to area 45), as well as in the left posterior midcingulate cortex (pMCC), dorsal posterior cingulate cortex (dPCC), frontal operculum, and sublenticular part of the basal forebrain (Ch4).

p24c was associated with 7 co-activation clusters (Fig. 5B, Table 3). Maxima were located mainly in cortical regions and, in contrast to p24ab co-activations, were predominantly left-lateralized. Cortical bilateral maxima were found in the anterior insula and middle frontal gyrus (dorsal and rostral to area 45), as well as in the frontal operculum, whereas subcortically they were restricted to the caudate nucleus. Right-lateralized maxima were found in area 45, the anterior midcingulate cortex (aMCC), and MDpr. Maxima restricted to the left hemisphere

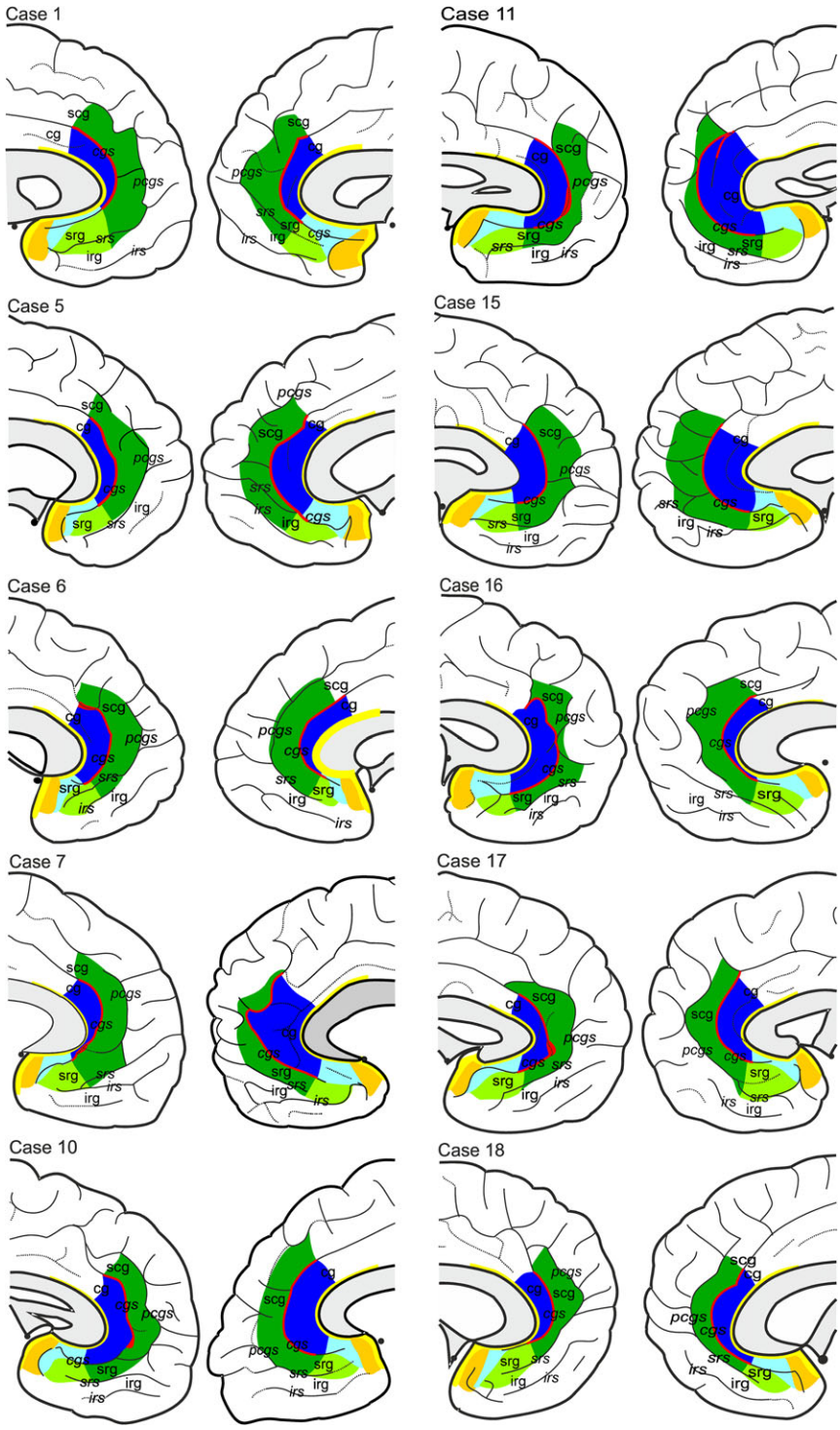

Figure 2. Schematic drawings depicting the extent of p24ab (in dark blue), p24c (in red), and p32 (in dark green) in each of the 10 postmortem cases examined in the present study and their relationship to macroanatomical landmarks and previously described (Palomero-Gallagher et al. 2015) subgenual anterior cingulate areas 25 (in orange), s24 (in pale blue), and s32 (in pale green) as well as area 33 (in yellow). Dotted lines indicate dimples, i.e., extremely shallow sulci. Note that p24c was only visible on the surface when the sulcus was interrupted or became very shallow. Since this only occurred in the left hemisphere of cases 10, 11, and 17, p24c is mostly only depicted as a thin line representing its extent within the cingulate sulcus. Sulci are labeled in italics, gyri in regular fonts. cg: cingulate gyrus; cgs: cingulate sulcus; irg: inferior rostral gyrus; irs: inferior rostral sulcus; scg: superior cingulate gyrus; srg: superior rostral gyrus; srs: superior rostral sulcus. Black circles indicate the position of the anterior commissure.

were found on the medial frontal gyrus rostral to the primary motor cortex (i.e., in the premotor cortex), on the precentral gyrus at the junction between the inferior frontal and the inferior precentral sulci (area ifj2), in the intraparietal (area hIP3) and inferior frontal sulci, as well as in Ch4 and the ventral striatum.

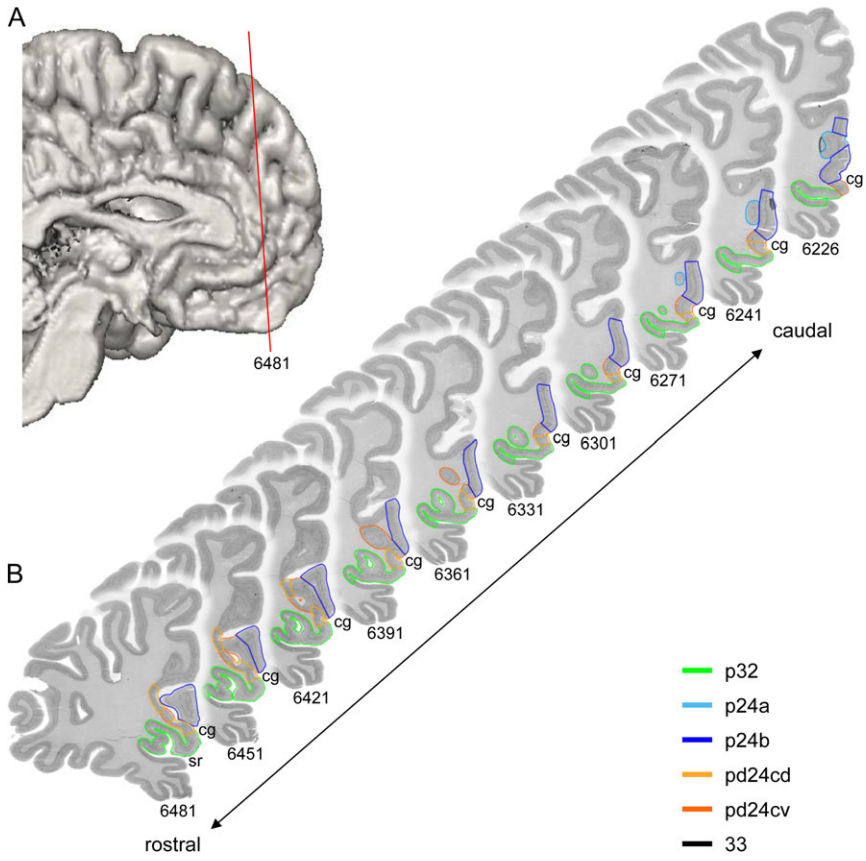

Figure 3. (A) Mesial surface of the left hemisphere of case 11. Red line marks the position of section 6481. (B) Anterior–posterior sequence of 10 coronal histological sections through the left hemisphere of case 11 showing cytoarchitectonically defined areas within pACC. Spacing between sections is 600 μm in all cases except for section 6226, which is only separated by 300 μm from section 6241. Note that different parts of area 24c are only visible on the surface when the cingulate sulcus becomes as shallow as a dimple. cg: cingulate sulcus; sr: superior rostral sulcus.

Table 2 Mean (in mm^3 ± SD) absolute histological volumes of pACC areas before (normal font) and after (italics) correction for total brain size.

	p24ab	p24c	p32
Left hemisphere ± SD	680 ± 271	603 ± 195	2918 ± 447
	0.052 ± 0.018	*0.046 ± 0.010*	*0.227 ± 0.037*
Right hemisphere ± SD	663 ± 228	711 ± 92	3107 ± 539
	0.050 ± 0.013	*0.055 ± 0.007*	*0.241 ± 0.038*
Male brains ± SD	862 ± 164	758 ± 111	3235 ± 582
	0.062 ± 0.012	*0.054 ± 0.007*	*0.233 ± 0.046*
Male brains, left hemisphere ± SD	896 ± 120	756 ± 161	3004 ± 593
	0.065 ± 0.011	*0.054 ± 0.008*	*0.216 ± 0.044*
Male brains, right hemisphere ± SD	828 ± 207	760 ± 43	3467 ± 525
	0.059 ± 0.013	*0.055 ± 0.007*	*0.251 ± 0.046*
Female brains ± SD	481 ± 135	557 ± 135	2790 ± 250
	0.040 ± 0.010	*0.047 ± 0.011*	*0.235 ± 0.028*
Female brains, left hemisphere ± SD	464 ± 187	451 ± 46	2832 ± 283
	0.039 ± 0.014	*0.038 ± 0.002*	*0.238 ± 0.029*
Female brains, right hemisphere ± SD	497 ± 73	662 ± 106	2747 ± 236
	0.042 ± 0.007	*0.055 ± 0.007*	*0.231 ± 0.030*

Data are presented as mean values computed for areas of the left and right hemispheres (independent of gender), or from male and female donors (after summing volumes from both hemispheres, or independently for the left and right hemisphere). Volumes were measured in the reconstructed histological brain volumes prior to spatial normalization and were individually corrected for shrinkage concomitant of histological processing.

p32 presented the most widespread pattern of co-activated clusters, which were often lateralized, and mainly located in the cerebral cortex (Fig. 5C, Table 3). Bilateral maxima were restricted to area 45, the inferior rostral sulcus (rostral to area 45), the medial frontal gyrus, the laterobasal (LB) nucleus of the amygdala, and the caudate nucleus. Within the thalamus, maxima were found in the right MDpr and the left portion of the mediodorsal thalamic nucleus connected with the temporal

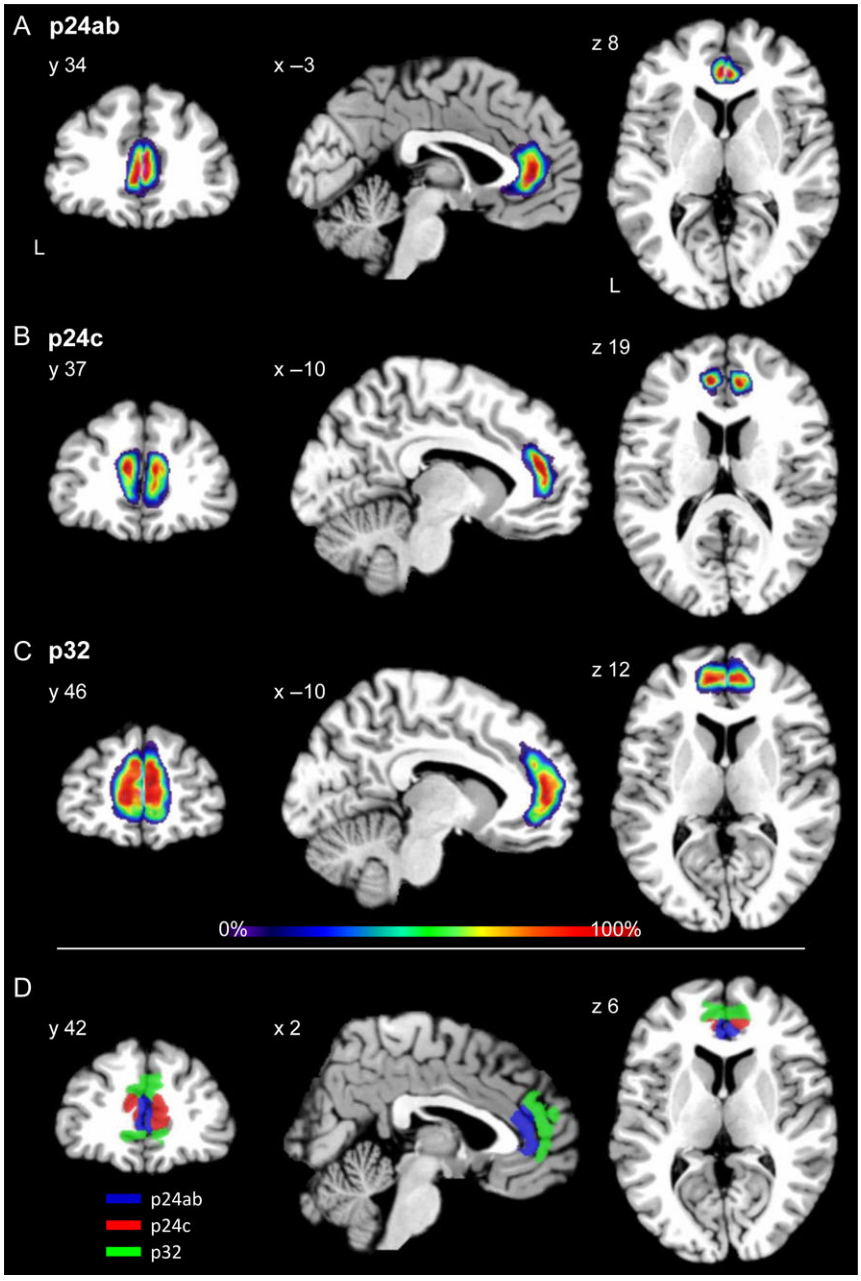

Figure 4. Sections through the MNI single-subject template (Evans et al. 2012) showing the continuous (*A–C*) and maximum (*D*) probability maps of p24ab (blue in *D*), p24c (red in *D*), and p32 (green in *D*) in the coronal, sagittal, and horizontal planes of sectioning. The number of overlapping brains in the continuous probability maps is color coded according to the scale bar. Scale bar encodes overlap probability from low brains (10%) up to high probabilities in dark red (10 out of 10 brains, 100%). Note that area p24c is not visible on the view of the mesial surface of the hemisphere because it is buried in the cingulate sulcus. L: left hemisphere.

cortex (MDt). The putamen and hypothalamus also presented lateralized maxima, which were located only in the right hemisphere, In contrast, all lateralized cortical maxima were found in the left hemisphere, and included frontopolar area Fp1, dorsolateral prefrontal cortex, anterior insula, inferior parietal area PGp, pMCC, and vPCC.

Conjunction analyses revealed a certain degree of overlap of the co-activation networks of p24ab, p24c, and p32 (Table 4). p24ab and p24c presented common co-activation clusters bilaterally only in the anterior insula and ventral striatum. Left-lateralized maxima were identified in Fp1, frontal operculum, Ch4 and putamen, whereas right-lateralized maxima were found in the inferior frontal sulcus (rostral to area 45), aMCC, and the medial frontal gyrus (rostral to the premotor cortex), the caudate and MDpr. Areas p24ab and p32 had 7 common co-activation clusters. Bilateral maxima were found in the anterior insula, ventral striatum, putamen, and MDpr. Left-lateralized maxima were restricted to the cingulate cortex (pMCC, dPCC, and vPCC), the Ch4 and the hypothalamus. Maxima in the right hemisphere were located in area 45, the dorsolateral prefrontal cortex, aMCC, the superficial group of amygdalar nuclei (SF), the LP/Pu complex, and the caudate nucleus. Finally, functional networks of p24c and p32 overlapped bilaterally in the anterior insular cortex, the caudate nucleus and the thalamus (MDpr and MDt). Common

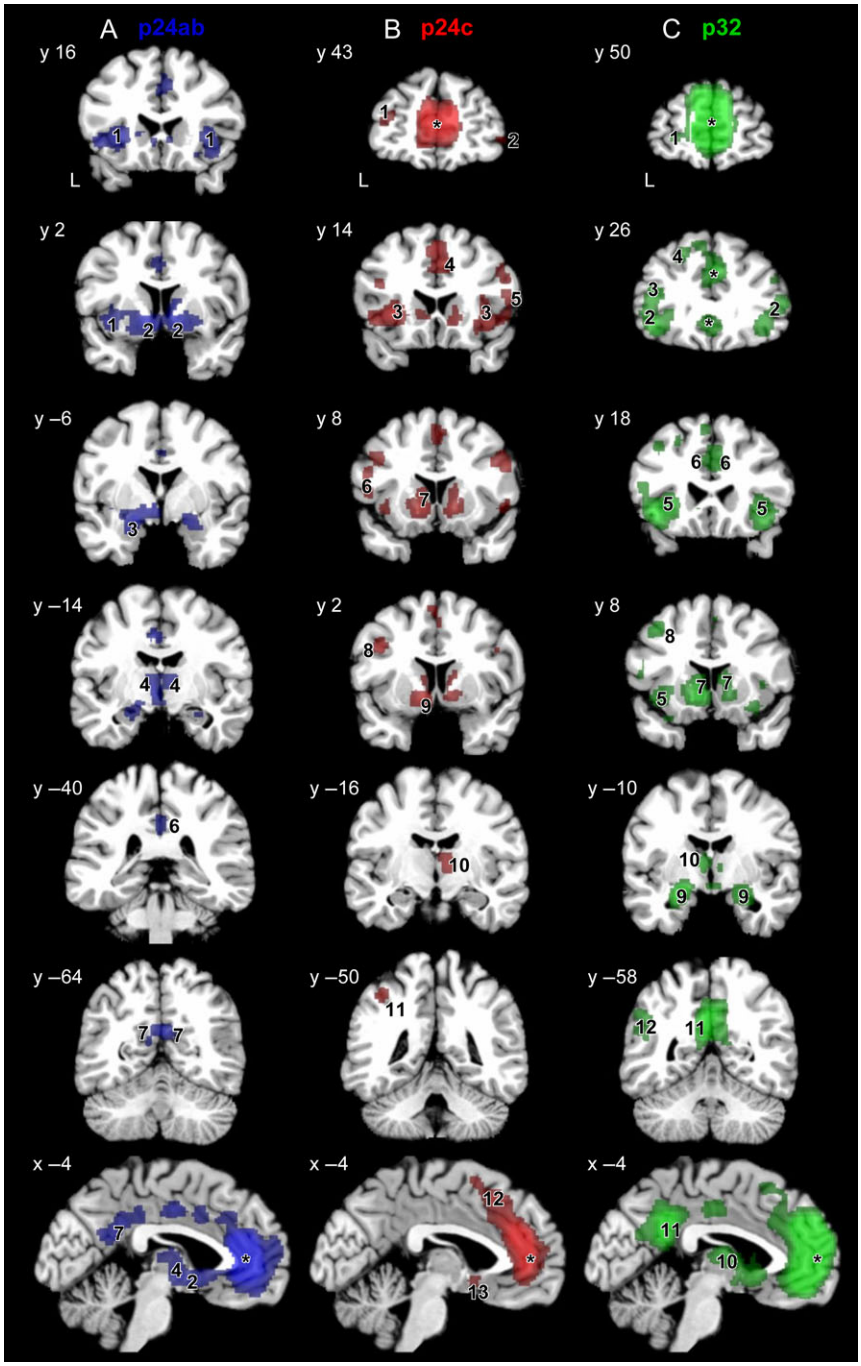

Figure 5. Functional connectivity patterns of p24ab (*A*), p24c (*B*), and p32 (*C*) displayed on the MNI single-subject template (Evans et al. 2012). Numbers indicate significant maxima within a specific cluster. Area p24ab: anterior insula (1), ventral striatum (2), sublenticular portion of the basal forebrain (Ch4, 3), portion of the mediodorsal thalamic nucleus connected with the prefrontal cortex (MDpr, 4), posterior midcingulate cortex (pMCC, 5), dorsal posterior cingulate cortex (dPCC, 6), and ventral posterior cingulate cortex (vPCC, 7). Area p24c: middle frontal gyrus (1), inferior frontal sulcus as it as it swings down rostral to the horizontal branch of the Sylvian fissure (2), anterior insula (3), aMCC (4), area 45 (5), area 44 (6), caudate nucleus (7), area ifj2 (8), ventral striatum (9), portion of the mediodorsal thalamic nucleus connected with the prefrontal cortex (MDpr, 10), intraparietal area 3 (hIP3, 11), premotor cortex (12), and sublenticular portion of the basal forebrain (Ch4, 13). Area p32: frontopolar area Fp1 (1), area 45 (2), the inferior frontal sulcus (3), the superior frontal sulcus (4), anterior insula (5), medial frontal gyrus (6), caudate nucleus (7), middle frontal gyrus (8), laterobasal nucleus of the amygdala (LB, 9), LP/Pu (10), ventral posterior cingulate cortex (vPCC, 11), posterior inferior parietal area PGp (12). Stereotaxic coordinates are given in anatomical MNI space (Amunts et al. 2005). Cluster sizes and assignations are specified in Table 3. L: left hemisphere. Asterisks indicate cluster surrounding the seed region. Note, that only significant maxima have been identified and labeled.

maxima in the left hemisphere were found in area Fp1, the medial frontal gyrus (rostral to premotor cortex), Ch4 (Nucl. Basalis Meynert), and the ventral striatum. Those in the right hemisphere were located in area 45, the premotor cortex, globus pallidus, and putamen.

The contrast analyses revealed that p24ab showed stronger co-activations with the claustrum, basal ganglia, and hypothalamus than did p24c or p32 (Fig. 6A and *B*, Table 5). Additionally, p24ab was more strongly associated with the basal forebrain and amygdala than was p24c (Fig. 6A). In contrast, weaker

Table 3 Functional co-activation clusters for p24ab, p24c, and p32.

Macroanatomical location	Hemisphere	Cytoarchitectonic area/*brain region*	Cluster size [voxel]	Anatomical MNI		
				x	y	z
p24ab						
Basal ganglia	L	*Globus pallidus*	9095	−8	2	−3
Insular lobe	L	*Anterior insula*		−32	16	5
Insular lobe	R	*Anterior insula*		36	12	5
Basal forebrain	L	Ch4 [30%]		−20	−6	−9
Basal ganglia	R	*Globus pallidus*		10	2	−1
Thalamus	R	MDpr [66%]		6	−20	13
Thalamus	L	MDpr [82%]		−6	−12	3
Insular lobe	L	*Anterior insula*		−38	8	−3
Cingulate gyrus	L	*pMCC*		−6	−14	45
Inferior frontal gyrus	L	*Frontal operculum*		−46	16	1
Precuneus	R	*vPCC*	763	2	−64	27
Precuneus	L	*vPCC*		−2	−52	35
Precuneus	L	*dPCC*		−2	−40	41
Calcarine sulcus	L			−10	−66	17
Middle frontal gyrus	R		208	46	32	21
Middle frontal gyrus	R			44	38	29
p24c						
Cingulate gyrus	R	*aMCC*	4405	4	18	41
Medial frontal gyrus	L			−2	16	51
Medial frontal gyrus	L			0	24	47
Medial frontal gyrus	L	*Premotor*		−4	2	65
Medial frontal gyrus	L	*Premotor*		−2	4	63
Superior frontopolar gyrus	L	Fp1 [47%]		−8	58	19
Insular lobe	L	*Anterior insula*	1882	−32	18	5
Basal ganglia	L	*Ventral striatum*		−10	2	−3
Precentral gyrus	L	ifj2 [33%]		−42	2	37
Inferior frontal gyrus	L	*Frontal operculum*		−48	16	1
Basal forebrain	L	Ch4 [44%]		−18	−8	−7
Basal ganglia	L	*Caudate nucleus*		−12	8	9
Inferior frontal gyrus	L	44 [68%]		−52	8	13
Inferior frontal gyrus	L	44 [55%]		−54	8	19
Inferior frontal sulcus	L			−44	14	27
Basal ganglia	L	*Caudate nucleus*		−10	−4	13
Inferior frontal gyrus	R	*Frontal operculum*	727	50	38	1
Inferior frontal gyrus	R	*WM*		52	10	31
Middle frontal gyrus	R			46	32	27
Inferior frontal gyrus	R	*Pars opercularis*		46	8	35
Inferior frontal gyrus	R	*Pars triangularis*		48	30	9
Insular lobe	R	*Anterior insula*	708	40	18	−3
Inferior frontal gyrus	R	*Frontal operculum*		52	12	1
Insular lobe	R	*Anterior insula*		36	16	9
Inferior frontal gyrus	R	45 [42%]		54	14	17
Inferior frontal gyrus	R	*WM*		36	28	5
Basal ganglia	R	*Caudate nucleus*	683	12	10	−1
Thalamus	R	MDpr [87%]		8	−16	9
Basal ganglia	R	*Caudate nucleus*		14	4	11
Inferior frontal sulcus	L		147	−44	36	13
Middle frontal gyrus	L			−36	48	11
Middle frontal gyrus	L			−38	42	17
Intraparietal sulcus	L	hIP3 [36%]	139	−42	−50	53
p32						
Superior frontal gyrus	L	*WM*	7429	−18	50	9
Superior frontal sulcus	L			−24	26	47
Superior frontal sulcus	L			−22	28	49
Superior frontal gyrus	L			−14	32	53
Frontal pole	L	*WM*		−18	48	1
Superior frontal gyrus	L	*WM*		−20	46	5
Superior orbital gyrus	L	Fp1 [63%]		−28	48	3
Medial frontal gyrus	L			−4	16	61
Medial frontal gyrus	R			2	12	59
Amygdala	L	LB [38%]	4184	−24	−10	−13

(*Continued*)

Table 3 (Continued)

Macroanatomical location	Hemisphere	Cytoarchitectonic area/*brain region*	Cluster size [voxel]	Anatomical MNI		
				x	y	z
Inferior frontal gyrus	L	*WM*		−44	22	−3
Insular lobe	L	*Anterior insula*		−32	22	−4
Basal ganglia	L	*Caudate nucleus*		−8	8	−1
Inferior frontal sulcus	L	*IFS/pars triangularis*		−44	26	19
Thalamus	L	MDt [57%]		−4	−16	13
Thalamus	L	MDt [61%]		−6	−8	9
Thalamus	R	MDt [94%]		10	−20	7
Inferior frontal gyrus	L	45 [27%]		−52	18	15
Hypothalamus	R			4	−10	−7
Insular lobe	L	*Anterior insula*		−32	6	−19
Precuneus	L	*vPCC*	1863	−4	−54	35
Cuneus	L			−4	−72	27
Inferior frontal sulcus	R	*Frontal operculum*	1228	38	20	−3
Inferior frontal gyrus	R	45 [54%]		54	26	11
Inferior frontal sulcus	R	*IFS/pars triangularis*		46	32	31
Inferior frontal sulcus	R	*IFS/pars triangularis*		48	24	29
Amygdala	R	LB [48%]	779	24	−6	−15
Basal ganglia	R	*Caudate nucleus*		10	4	13
Basal ganglia	R	*Caudate nucleus*		14	8	−1
Basal ganglia	R	*Putamen*		22	0	1
Angular gyrus	L	PGp [34%]	769	−48	−68	33
Cingulate gyrus	L	*pMCC*	246	0	−22	45
Middle frontal gyrus	L		229	−42	10	49

Cluster maxima were assigned to most probable cytoarchitectonic area when present in the SPM Anatomy Toolbox (Eickhoff et al. 2005). Brain regions (in italics) or cytoarchitectonically defined areas were identified based on previously published criteria: 44 and 45 (areas 44 and 45 of Broca's region; (Amunts et al. 1999), aMCC (anterior portion of the midcingulate cortex, encompasses areas a24' and 32'; (Vogt et al. 2003; Palomero-Gallagher et al. 2009), anterior insular region (Kurth et al. 2010), Ch4 (sublenticular part of the basal forebrain; (Zaborszky et al. 2008), dPCC (dorsal posterior cingulate cortex; encompasses areas 23d, d23, and 31; (Vogt et al. 2006), Fp1 (frontopolar area Fp1; (Bludau et al. 2014), frontal operculum (includes opercular areas op4-op9; (Amunts et al. 2010), hIP3 (area 3 on the medial wall of the intraparietal sulcus; (Scheperjans, Eickhoff et al. 2008; Scheperjans, Hermann et al. 200 8), ifj2 (area 2 at the inferior frontal junction region; (Amunts et al. 2010), IFS (inferior frontal sulcus), LB (laterobasal nucleus of the amygdala; (Amunts et al. 2005), MDpr and MDt (parts of the mediodorsal thalamic nucleus connected with the prefrontal and temporal cortices, respectively; (Behrens et al. 2003), pMCC (posterior portion of the midcingulate cortex, encompasses areas p24' and 24d; (Vogt et al. 2003; Palomero-Gallagher et al. 2009), premotor (premotor cortex, encompasses the rostral and caudal supplementary motor areas; (Zilles et al.1996), vPCC (ventral posterior cingulate cortex; encompasses areas v23 and 31; (Vogt et al. 2006), WM (white matter). Coordinates are given in anatomical MNI space (Amunts et al. 2005).

co-activations of p24ab than of either p24c or p32 were restricted to the cerebral cortex. p24c was found to be more strongly activated with area 45 and the premotor cortex in the right hemisphere, as well as with areas 44, ifj2, hIP2, and hIP3 in the left hemisphere than was p24ab. Furthermore, p24ab was more strongly associated with the anterior insula in the left hemisphere than was p24c, and the opposite holds true for the right hemisphere. p24ab and p24c presented a differential connectivity with the cingulate cortex. Specifically, p24ab showed stronger co-activation patterns with areas s24 and p32 of the anterior cingulate cortex as well as with vPCC pMCC, but a weaker association with aMCC than did p24c. When comparing the cortical co-activation patterns of p24ab and p32 (Fig. 6B, Table 5), the former was found to be more strongly activated with the anterior insula (bilaterally), and the latter with area 45 on the right hemisphere as well as with inferior parietal areas PFm, PGa and PGp on the left hemisphere. p24ab and p32 also presented a differential connectivity with the cingulate cortex, since p24ab was more strongly associated with aMCC, pMCC and dPCC in the left hemisphere, and p32 with vPCC in the right hemisphere. Contrast analyses between p24c and p32 revealed a more widespread network for the former area (Fig. 6C, Table 5). p24c presented stronger co-activations than p32 in the anterior insula, putamen and globus pallidus bilaterally, in area 45, the aMCC, caudate nucleus, MDpr, and MDt of the right hemisphere, as well as in areas 44, ifj2, hIP2, and hIP3, and in the premotor cortex of the left hemisphere. Stronger activations of p32 than of p24c were found in the superior frontal gyrus, frontal operculum laterobasal amygdalar nuclei and the cornu ammonis region 1 (CA1) of the hippocampus.

Functional Characterization of sACC Areas

A functional decoding analysis based on the BrainMap metadata was performed to outline the functional profiles of the seed volumes of interest defined by the MPMs of p24ab, p24c, and p32. Furthermore, we determined the functional domains and Paradigm Classes with which they could be significantly associated (Fig. 7). As specified in the Material and Methods section, results were only considered robust in the case of congruent forward and reverse inferences.

All 3 areas were significantly associated with the Behavioural Domains of emotion (i.e., the mental faculty of experiencing an affective state of consciousness) and cognition (i.e., mental process of knowing, including the integration of awareness, perception, reasoning, and judgment) and were activated by paradigms involving monitoring and decision making, such as the reward task (Fig. 7). Only p24ab was specifically associated with the perception of taste and the awareness of physiological sensations specifically related to sexuality, although both p24ab and p24c were activated by tasks involving taste. Only p24c was significantly linked with the ability to prevent any form of planned

Table 4 Stereotaxic coordinates (specified in anatomical MNI space) of clusters revealed by the conjunction analyses.

Macroanatomical location	Hemisphere	Cytoarchitectonic area/*brain region*	Cluster size [voxel]	Anatomical MNI		
				x	y	z
p24ab + p24c						
Cingulate gyrus	R	*aMCC*	2797	4	16	43
Medial frontal gyrus	R			2	12	49
Superior frontopolar gyrus	L	Fp1 [47%]		−8	58	19
Insular lobe	L	*Anterior insula*	1265	−32	16	5
Basal ganglia	L	*Ventral striatum*		−10	2	−3
Basal ganglia	L	*Putamen*		−12	6	−1
Inferior frontal gyrus	L	*Frontal operculum*		−46	16	1
Basal forebrain	L	Ch4 [44%]		−18	−8	−7
Basal ganglia	R	*Ventral striatum*	316	12	6	−1
Basal ganglia	R	*Caudate nucleus*		12	2	13
Capsula interna	R			8	−2	7
Insular lobe	R	*Anterior insula*	257	38	16	−1
Insular lobe	R	*Anterior insula*		38	16	9
Thalamus	R	MDpr [76%]	183	8	−16	11
Medial frontal gyrus	R		130	46	30	25
Middle frontal gyrus	R			44	38	29
Inferior frontal sulcus	R	*IFS/pars triangularis*		46	32	13
p24ab + p32						
Cingulate gyrus	R	*aMCC*	3370	2	18	41
Gyrus rectus	R			2	32	−15
Insular lobe	L	*Anterior insula*	2259	−32	16	5
Basal ganglia	L	*Ventral striatum*		−10	2	−3
Basal forebrain	L	Ch4 [44%]		−20	−6	−9
Insular lobe	L	*Anterior insula*		−38	10	−3
Inferior frontal gyrus	L	*Frontal operculum*		−46	16	1
Thalamus	L	MDpr [88%]		−8	−12	9
Thalamus	R	MDt [55%]		2	−18	13
Thalamus	R	MDpr [93%]		10	−20	9
Thalamus	L	MDpr [91%]		−6	−24	11
Hypothalamus	L			−2	−8	−7
Basal ganglia	L	*Putamen*		−34	−2	1
Precuneus	L	*vPCC*	639	−2	−52	35
Precuneus	L	*dPCC*		0	−62	27
Precuneus	L	*dPCC*		−2	−42	41
Amygdala	R	SF [31%]	459	22	−8	−13
Basal ganglia	R	*Caudate nucleus*		10	4	7
Basal ganglia	R	*Ventral striatum*		14	8	−1
Basal ganglia	R	*Putamen*		22	0	1
Insular lobe	R	*Anterior insula*	309	38	16	1
Insular lobe	R	*Anterior insula*		28	14	−11
Cingulate gyrus	L	*pMCC*	99	−2	−18	43
Inferior frontal gyrus	R	45 [34%]	56	48	32	15
Middle frontal gyrus	R			46	32	27
Inferior frontal gyrus	R	45 [34%]		48	26	27
Middle frontal gyrus	R			44	36	31
p24c + p32						
Medial frontal gyrus	L		3271	−4	26	53
Medial frontal gyrus	L	Fp1 [47%]		−8	58	19
Insular lobe	L	*Anterior insula*	1364	−32	18	3
Basal ganglia	L	*Ventral striatum*		−10	2	−3
Inferior frontal gyrus	L	*Frontal operculum*		−48	18	1
Basal forebrain	L	Ch4 [44%]		−18	−8	−7
Basal ganglia	L	*Caudate nucleus*		−12	8	9
Thalamus	L	LP/Pu [42%]		−8	−6	11
Basal ganglia	L	*Caudate nucleus*		−10	−4	13
Thalamus	L	MDpr [98%]		−10	−10	9
Thalamus	L	MDpr [88%]		−8	−10	5
Insular lobe	R	*Anterior insula*	415	40	18	−3
Insular lobe	R	*Anterior insula*		38	16	7

(*Continued*)

Table 4 (Continued)

Macroanatomical location	Hemisphere	Cytoarchitectonic area/*brain region*	Cluster size [voxel]	Anatomical MNI		
				x	y	z
Basal ganglia	R	*Caudate nucleus*	234	12	8	7
Basal ganglia	R	*Caudate nucleus*		14	4	11
Basal ganglia	R	*Putamen*		14	8	−1
Basal ganglia	R	*Globus pallidus*		10	4	5
Basal ganglia	R	*Caudate nucleus*		8	−2	9
Inferior frontal gyrus	R	*Pars triangularis*	125	46	32	31
Inferior frontal gyrus	R	45 [29%]		50	28	9
Inferior frontal gyrus	R	45 [30%]		48	32	13
Inferior frontal gyrus	R	45 [32%]		46	32	17
Inferior frontal gyrus	R	45 [25%]		48	26	29
Thalamus	R	MDpr [92%]	110	8	−18	9
Thalamus	R	MDt [68%]		4	−18	13
Medial frontal gyrus	R	*Premotor*	75	2	12	59
Medial frontal gyrus	L			−4	18	57
Medial frontal gyrus	L			−6	20	55

Cluster maxima assigned to most probable cytoarchitectonic area when present in the SPM Anatomy Toolbox (Eickhoff et al. 2005). Brain regions (in italics) or cytoarchitectonically defined areas were identified based on previously published criteria: 45 (area 45 of Broca's region; Amunts et al. 1999), aMCC (anterior portion of the midcingulate cortex, encompasses areas a24' and 32'; Vogt et al. 2003; Palomero-Gallagher et al. 2009), anterior insular region (Kurth et al. 2010), Ch4 (sublenticular part of the basal forebrain; Zaborszky et al. 2008), dPCC (dorsal posterior cingulate cortex; encompasses areas 23d, d23, and 31; Vogt et al. 2006), Fp1 (frontopolar area Fp1; Bludau et al. 2014), frontal operculum (includes opercular areas op4-op9; Amunts et al. 2010), IFS (inferior frontal sulcus), MDpr and MDt (parts of the mediodorsal thalamic nucleus connected with the prefrontal and temporal cortices, respectively; Behrens et al. 2003), pMCC (posterior portion of the midcingulate cortex, encompasses areas p24' and 24d; Vogt et al. 2003; Palomero-Gallagher et al. 2009), premotor (premotor cortex, encompasses the rostral and caudal supplementary motor areas; Zilles et al.1996), SF (superficial group of amygdala nuclei; Amunts et al. 2005), vPCC (ventral posterior cingulate cortex; encompasses areas v23 and 31; Vogt et al. 2006). Coordinates are given in anatomical MNI space (Amunts et al. 2005).

motor response. Only p32 was associated with the more specific domains of emotion pertaining the processing of anxiety or fear, and those of cognition related to the individual's ability to engage in social interactions, as well as to perceive, evaluate, respond to, and communicate in a language about bodily sensations, feelings, thoughts and experiences (Fig. 7). Indeed, p32 was activated by the theory of mind task, which probes the volunteer's ability to understand the personal beliefs and feelings of another person, or form hypotheses regarding the mental states of others. Furthermore, p32 was not only involved in emotion induction tasks, but was also activated by cognitive processes associated with monitoring and decision making such as the reward, episodic recall, and lexical decision tasks.

Surprisingly, we did not find a significant association between any of the pACC areas and the subjective state of pleasure, although at the time of the study the BrainMap database contained a total of 124 studies reporting tasks belonging to the behavioral domain happiness. However, only a very small number of these experiments reported activation foci within p24ab, p24c, and/or p32. Specifically, 5 of these studies (encompassing 81 subjects and 32 activation foci) reported activations within p24ab, 2 studies (encompassing 55 subjects and 24 activation foci) involved p24c, and 10 studies (encompassing 140 subjects and 87 activation foci) found activation within p32.

Discussion

The present study provides the first probability maps in stereotaxic space of cytoarchitectonic areas p24ab, p24c, and p32, which were previously identified based on observer-independent quantitative criteria (Palomero-Gallagher et al. 2008), and sheds new light on the functions of the pACC region based on the results of a database-driven meta-analytic connectivity modeling and quantitative functional decoding approach. We generated continuous and MPMs of areas p24ab (encompassing gyral cytoarchitectonic areas p24a and p24b), p24c (encompassing cytoarchitectonic areas pv24c, pd24cv and pd24cd of the cingulate sulcus) and p32 (covers cytoarchitectonic area p32). Each of the MPMs was then used as a seed volume for a database-driven analysis of task-dependent functional connectivity and functional decoding in order to infer the area's functions and its interactions with other brain regions. Areas p24ab and p24c shared a common functional profile involving the cognition and emotion Behavioural Domains, and were activated by reward tasks. Area p24a was specifically associated with the domains of gustation and interoception, and p24c with that of action inhibition. Additionally, p32 was associated with the specific domains of social cognition, anxiety and fear, and was specifically activated by paradigms probing for emotion induction and theory of mind. Notably, we did not find a significant association between any of the pACC areas and the subjective state of pleasure. Meta-analytic connectivity modeling revealed significant differences in the co-activation patterns of the 3 areas. p24ab presented the most restricted co-activation pattern, but also the strongest association with subcortical structures, and p24c had the most widespread functional connectivity pattern. Additionally, all 3 areas were found to be co-activated with components of the executive (Seeley et al. 2007), and default mode (Greicius et al. 2003; Fox, Snyder, et al. 2005; Fransson and Marrelec 2008) networks. Additionally, we could demonstrate that p24ab and p24c co-activated with elements of the salience network (Seeley et al. 2007), p24ab with parts of the affective network (George et al. 1995; Lévesque et al. 2003), and p32 with regions belonging to the cognitive (Seeley et al. 2007) and theory of mind (Abu-Akel and Shamay-Tsoory 2011; Schurz et al. 2014; Spunt and Adolphs 2017) networks.

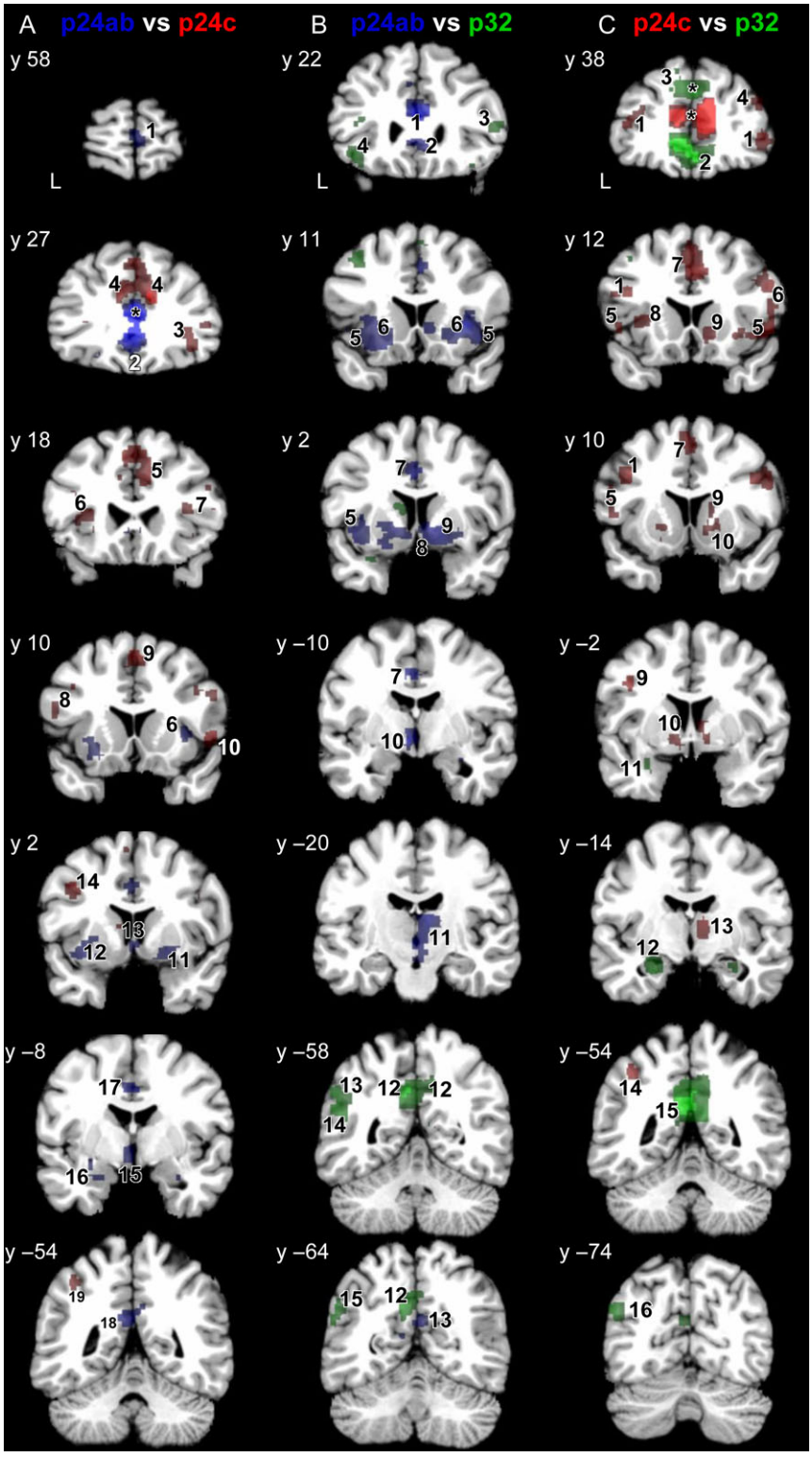

Figure 6. Clusters revealed by the contrasts analysis between p24ab and p24c (A; clusters more strongly associated with p24ab than with p24c are coded in blue, those more strongly associated with p24c than with p24ab in red), p24ab and p32 (B; clusters more strongly associated with p24ab than with p32 are coded in blue, those more strongly associated with p32 than with p24ab in green) as well as p24c and p32 (C; clusters more strongly associated with p24c than with p32 in red, those more strongly associated with p32 than with p24c are coded in green) displayed on the MNI single-subject template (Evans et al. 2012). Numbers indicate significant clusters. Areas p24ab and p24c: frontopolar area Fp2 (1), subgenual cingulate area s24 (2), the frontal operculum (3), the medial frontal gyrus (4), the aMCC, (5), the anterior insula (6), area 45 (7), area 44 (8), the premotor cortex (9), the inferior frontal sulcus (10), the putamen (11), the claustrum (12), magnocellular nuclei of the basal forebrain (Ch1-3, 13), area ifj2 (14), the hypothalamus (15), the laterobasal nucleus of the amygdala (LB, 16), the posterior midcingulate cortex (pMCC, 17), ventral posterior cingulate cortex (vPCC, 18), and intraparietal area 2 (hIP2, 19). Areas p24ab and p32: aMCC (1), area 33 (2), area 45 (3), lateral orbital gyrus (4), anterior insula (5), putamen (6), posterior midcingulate cortex (pMCC, 7), ventral striatum (8), globus pallidus (9), hypothalamus (10), portion of the mediodorsal thalamic nucleus connected

We found no interhemispheric or gender differences in the size of pACC areas after correction for differences in total brain size. These volumetric findings are difficult to correlate with previous results from the literature, because they mostly report data obtained from the portion of the cingulate gyrus which covers the pACC and the MCC portions of the cingulate gyrus (e.g., Makris et al. 2010; Seidman et al. 2006), or with regions of interest restricted to the perigenual portion of the cingulate gyrus, but covering the entire cingulate gyrus (e.g., Sturm et al. 2013), and thus cover our area p24ab together with the portion of our p24c located on the posterior/ventral bank of the cingulate gyrus. Furthermore, although in their Table 3, Sturm et al. (2013) report a larger volume of their region of interest in the left than in the right hemisphere (1722.9 ± 329.8 vs. 2310 ± 449.4 mm^3), they did not specify whether this result was significant.

The pACC and Happiness

Contrary to the view that the pACC subserves the processing of happiness and sACC that of sadness (Vogt et al. 2003), we did not find any cytoarchitectonic subdivision of pACC to be *significantly* linked to positively valenced emotions. Our results should not be interpreted in the sense that the pACC region is not *involved* in the processing of happiness, since when we specifically queried the BrainMap database for tasks belonging to the behavioral domain "happiness", we found a total of 124 studies. However, only 5 of them reported activations within p24ab, 2 involved p24c, and 10 found a activations within p32, and there was not a significant convergence of activations within pACC areas compared with those located in other brain regions. Our results are in accordance with several previously published meta-analytic studies using quantitative or traditional literature search strategies which also failed to allocate the processing of positively valenced emotions to a specific cingulate region, or even to the cingulate gyrus (e.g., Phan et al. 2002; Vytal and Hamann 2010; Torta and Cauda 2011; Kirby and Robinson 2017). Thus, although the pACC by all means participates in the processing of positively valenced emotions, it cannot be categorized as being a "central hub" (van den Heuvel and Sporns 2013) in the network processing happiness (Salzman and Fusi 2010). The present result also highlights the advantage of the MACM approach agnostic to the focus of included experiments in contrast to meta-analyses which rely on a literature search for relevant publications by means of specific functional keywords pertaining to the research question. Whereas the latter approach is inherently selective and thus limited in its' generalizability, the former provides a more comprehensive functional characterization of brain regions (Eickhoff and Bzdok 2013) given that the BrainMap database is currently one of the most comprehensive neuroimaging databases. Finally, although a clear-cut attribution of a cognitive function to a Behavioural Domain or Paradigm Class is often difficult, as it might encompass a very wide range of concepts, attribution to subdomains (in our case that of "happiness") yields a much higher accuracy (Lancaster et al. 2012).

Functional Fingerprint and Connectivity of p24ab

Area p24ab was significantly associated with the global Behavioural Domains of cognition and emotion, as well as with the specific perception and interoception domains. It co-activated with components of the salience and executive-control (Seeley et al. 2007) networks such as the anterior insula, frontal operculum, and aMCC. Furthermore, p24ab was more strongly associated with the hypothalamus (included in the salience network; Seeley et al. 2007) than was p24c. It also co-activated with the PCC, a component of the default mode network (Greicius et al. 2003; Fox, Snyder, et al. 2005; Fransson and Marrelec 2008), and with areas Fp2, Fo1, s24, s32 and p32, which are part the affective network (George et al. 1995; Lévesque et al. 2003). These functional connectivity patterns and the association of p24ab with the Behavioural Domains of perception and interoception provide further evidence for the cross-talk taking place between ACC, the anterior insula, and the hypothalamus during the processing of bodily awareness and the control of neural homeostasis involving the sympathetic nervous system (Craig 2002, 2009). Furthermore, our results pinpoint p24ab as the specific cytoarchitectonic entity within the ACC subserving such functions. p24ab was also co-activated with the basal forebrain, the major source of cholinergic afferents to the cortex (Mufson et al. 2003). Although functional connectivity does not necessarily imply direct anatomical connections (Eickhoff and Grefkes 2011), in this case it may reflect direct input from the basal forebrain as determined by tracer studies in rhesus monkey (Koliatsos et al. 1988) and rodent (Zaborszky et al. 2015; Fillinger et al. 2017) brains. Furthermore, in the mouse brain it could be shown that areas 24a and 24b receive qualitatively similar input from the basal forebrain, albeit with different densities (Fillinger et al. 2017). Our results confirm, and expand, a previous study reporting a strong functional connectivity of the basal nucleus of Meynert and the ACC in humans (Li et al. 2014), and highlights the modulatory role of the cholinergic system on activity of brain regions controlling our motor response to the occurrence of salient stimuli.

Functional Fingerprint and Connectivity of p24c

Area p24c was significantly associated with the global Behavioural Domains of cognition and emotion, and with the specific action inhibition Behavioural Domain. It co-activated with diverse components of the salience and executive-control (Seeley et al. 2007) networks: anterior insula, frontal operculum, pMCC, inferior frontal gyrus (more extensively in the right than in the left hemisphere), and premotor cortex. The specific association of p24c with the action inhibition Behavioural Domain as well as its co-activation with the anterior insula and with multiple areas of the ventral prefrontal cortex, provide further support for the hypothesis that the inferior fontal gyrus is not the sole region implementing inhibitory control (Aron et al. 2004, 2014), but that activation of an extensive network is required for motor response inhibition (Levy and Wagner 2011; Hampshire and Sharp 2015). We also found p24c to co-activate with the ventral striatum, which is part of the salience, but not the executive network (Seeley et al. 2007),

with the temporal cortex (MDt, 11), ventral posterior cingulate cortex (dPCC, 12), as well as parietal areas PFm (13), PGa (14), and PGp (15). Areas p24c and p32: pars triangularis of the inferior frontal gyrus (1), gyrus rectus (2), superior frontal gyrus (3), middle frontal gyrus (4), area 44 (5), area 45 (6), premotor cortex (7), anterior insula (8), caudate nucleus (9), putamen (10), area ifj2 (11), globus pallidus (12), laterobasal nucleus of the amygdala (LB, 13), cornu ammonis region of the hippocampus (CA, 14), portion of the mediodorsal thalamic nucleus connected with the prefrontal cortex (MDpr, 15), intraparietal area 3 (hIP3, 16), ventral posterior cingulate cortex (vPCC, 17), and parietal area PGp (18). Stereotaxic coordinates are given in anatomical MNI space (Amunts et al. 2005). Cluster sizes and assignations are specified in Table 5. Asterisks indicate clusters surrounding the seed regions L: left hemisphere. Note, that only significant maxima have been identified and labeled.

Table 5 Stereotaxic coordinates (specified in anatomical MNI space) of clusters revealed by the contrasts analyses.

Macroanatomical location	Hemisphere	Cytoarchitectonic area/*brain region*	Cluster size [voxel]	Anatomical MNI		
				x	y	z
p24ab > p24c						
Cingulate gyrus	R	s24 [47%]	1844	2	28	−3
Superior frontopolar gyrus	R	Fp2 [78%]		4	58	11
Inferior rostral gyrus	L	s32 [11%]		−2	30	−15
Gyrus rectus	L	Fo1 [54%]		0	32	−17
Superior medial gyrus	R	p32 [62%]		4	52	23
Superior medial gyrus	R	p32 [56%]		4	50	27
Precuneus	R	*vPCC*	461	2	−64	27
Cuneus	L	hOc2 [28%]		−12	−66	19
Claustrum	L		300	−34	0	−7
Claustrum	L			−28	6	−5
Basal ganglia	L	*Putamen*		−30	6	1
Claustrum	L			−34	4	1
Cingulate gyrus	L	*pMCC*	209	−4	−14	41
Basal ganglia	R	*Putamen*	206	24	4	−3
Insular lobe	R	*Anterior insula*		34	10	5
Hypothalamus	L		172	−2	−8	−1
Basal forebrain	L	Ch1-3 [100%]		0	2	1
Hypothalamus	R			2	−16	−11
Amygdala	L	LB [40%]	68	−22	−12	−19
Thalamus	R	MDpr [28%]	61	2	−22	7
p24ab < p24c						
Medial frontal gyrus	L		2162	−4	22	51
Medial frontal gyrus	R	*Premotor*		4	10	57
Medial frontal gyrus	L			−8	18	51
Cingulate gyrus	R	*aMCC*		8	18	37
Medial frontal gyrus	R			8	22	51
Inferior frontal gyrus	R	*Pars triangularis*	189	52	38	5
Inferior frontal gyrus	R	*Frontal operculum*		52	30	5
Inferior frontal gyrus	R	*Frontal operculum*	157	52	12	3
Inferior frontal gyrus	R	45 [38%]		54	14	13
Inferior frontal gyrus	R	*Frontal operculum*	126	38	28	−1
Inferior frontal gyrus	R	*Frontal operculum*		38	30	3
Inferior frontal gyrus	R	45 [27%]	121	52	16	33
Inferior frontal sulcus	R	*IFS/pars opercularis*		48	16	39
Inferior frontal sulcus	R	*IFS/pars opercularis*		42	8	33
Inferior frontal sulcus	L	*IFS/pars triangularis*	112	−42	42	17
Middle frontal gyrus	L			−36	50	11
Insular lobe	L	*Anterior insula*	109	−34	20	11
Insular lobe	L	*Anterior insula*		−28	20	3
Precentral gyrus	L	ifj2 [35%]	105	−40	2	41
Intraparietal sulcus	L	hIP3 [41%]	101	−38	−50	57
Intraparietal sulcus	L	hIP2 [32%]		−44	−52	55
Inferior frontal gyrus	L	44 [59%]	53	−56	10	23
p24ab > p32						
Cingulate gyrus	R	s24 [38%]	2357	4	28	−3
Insular lobe	R	*Anterior insula*		36	12	5
Basal ganglia	R	*Ventral striatum*		10	0	−1
Basal ganglia	R	*Globus pallidus*		16	0	−3
Basal ganglia	R	*Putamen*		26	8	−1
Cingulate gyrus	R	33 [48%]		4	18	1
Basal ganglia	R	*Putamen*		20	6	−1
Insular lobe	R	*Anterior insula*		42	12	−5
Cingulate gyrus	L	*aMCC*		−8	24	39
Thalamus	R	MDt [52%]	1581	8	−20	15
Hypothalamus	L			−4	−12	−1
Claustrum	L			−22	6	−11
Insular lobe	L	*Anterior insula*		−30	8	−7
Insular lobe	L	*Anterior insula*		−44	0	−1
Insular lobe	L	*Anterior insula*		−38	0	13

(*Continued*)

Table 5 (Continued)

Macroanatomical location	Hemisphere	Cytoarchitectonic area/*brain region*	Cluster size [voxel]	Anatomical MNI		
				x	y	z
Basal ganglia	L	*Putamen*		−28	8	3
Cingulate gyrus	L	*pMCC*	330	−4	2	39
Cingulate gyrus	L	*pMCC*		−4	−8	43
Cingulate gyrus	L	*pMCC*		−6	−10	45
Middle frontal gyrus	R			2	10	43
Precuneus	L	*dPCC*	104	−2	−40	35
Precuneus	L	*dPCC*		0	−36	45
Inferior frontal gyrus	R	*Pars triangularis/IFS*	85	46	28	23
Precuneus	R	*vPCC*	79	2	−66	27
p24ab < p32						
Precuneus	L	*vPCC*	663	−6	−58	39
Precuneus	R	*vPCC*		12	−56	43
Precuneus	R	*vPCC*		2	−54	27
Supramarginal gyrus	L	PFm [55%]	377	−58	−58	39
Angular gyrus	L	PGa [46%]		−56	−60	31
Angular gyrus	L	PGa [49%]		−54	−58	29
Angular gyrus	L	PGp [54%]		−56	−70	35
Superior temporal sulcus	L			−46	−60	19
Inferior frontal gyrus	L		272	−46	28	−7
Lateral orbital gyrus	L			−40	16	−15
Middle frontal gyrus	L		174	−42	16	51
Inferior frontal gyrus	R	45 [47%]	70	54	22	13
p24c > p32						
Cingulate gyrus	R	*aMCC*	2606	4	16	41
Medial frontal gyrus	L			−2	16	51
Medial frontal gyrus	L	*Premotor*		−2	2	61
medial frontal gyrus	L	*Premotor*		−2	10	57
Thalamus	R	MDt [75%]	454	8	−20	17
Thalamus	R	MDt [40%]		8	−6	9
Basal ganglia	R	*Caudate nucleus*		12	14	−3
Thalamus	R	MDpr [57%]		4	−16	5
Basal ganglia	R	*Globus pallidus*		12	0	1
Basal ganglia	R	*Caudate nucleus*		16	6	13
Basal ganglia	R	*Putamen*		20	6	1
Basal ganglia	R	*Putamen*		18	6	7
Basal ganglia	R	*Caudate nucleus*		14	8	17
Insular lobe	L	*Anterior insula*	430	−34	18	7
Inferior frontal gyrus	L	44 [52%]		−52	14	3
Inferior frontal gyrus	L	*Pars opercularis*		−50	12	25
Inferior frontal gyrus	L	44 [56%]		−56	8	23
Inferior frontal gyrus	R	45 [41%]	399	54	14	31
Inferior frontal gyrus	R	*Pars opercularis*		42	8	33
Inferior frontal gyrus	R			52	30	27
Middle frontal gyrus	R			44	34	27
Middle frontal gyrus	R			48	16	41
Inferior frontal gyrus	R	44 [34%]	259	54	10	3
Insular lobe	R	*Anterior insula*		44	12	−3
Inferior frontal gyrus	R	45 [38%]		54	14	13
Insular lobe	R	*Anterior insula*		28	14	−3
Precentral gyrus	L	ifj2 [41%]	195	−44	4	35
Precentral gyrus	L	ifj2 [35%]		−42	0	37
Precentral gyrus	L			−46	0	37
Inferior frontal gyrus	L	*Pars triangularis*		−42	14	25
Inferior frontal gyrus	R	*Pars triangularis*	148	48	38	8
Intraparietal sulcus	L	hIP3 [54%]	139	−40	−52	53
Intraparietal sulcus	L	hIP2 [50%]		−50	−46	55
Middle frontal gyrus	L		139	−36	48	13
Inferior frontal gyrus	L	*Pars triangularis*		−46	38	15
Middle frontal gyrus	L			−36	44	19
Inferior frontal gyrus	R	*Pars triangularis*	125	36	28	7

(*Continued*)

Table 5 (Continued)

Macroanatomical location	Hemisphere	Cytoarchitectonic area/*brain region*	Cluster size [voxel]	Anatomical MNI		
				x	y	z
Inferior frontal gyrus	R	*Pars triangularis*		38	16	15
Basal ganglia	L	*Globus pallidus*	96	−12	−8	−1
Basal ganglia	L	*Globus pallidus*		−10	−4	−3
Basal ganglia	L	*Putamen*		−18	4	1
p24c < p32						
Gyrus rectus	R		3919	2	38	−11
Superior frontal gyrus	L			−12	34	51
Superior frontal gyrus	L			−14	36	53
Superior frontal gyrus	L			−18	50	7
Frontal lobe	L	WM		−18	48	1
Superior frontal gyrus	L			−20	46	5
Precuneus	L	*vPCC*	1434	−4	−56	25
Precuneus	L	*vPCC*		−4	−58	41
Angular gyrus	L	PGa [35%]	430	−54	−64	27
Angular gyrus	L	PGp [51%]		−54	−68	29
Angular gyrus	L	PGp [77%]		−52	−76	35
Angular gyrus	L	PGp [73%]		−54	−72	31
Hippocampus	L	CA [51%]	216	−26	−14	−21
Amygdala	L	LB [38%]		−32	−4	−21
Inferior frontal gyrus	L	*Frontal operculum*	109	−42	26	−7

Cluster maxima assigned to most probable cytoarchitectonic area when present in the SPM Anatomy Toolbox (Eickhoff et al. 2005). Brain regions (in italics) or cytoarchitectonically defined areas were identified based on previously published criteria: 33 (cingulate area 33; Palomero-Gallagher et al. 2008), 44 and 45 (areas 44 and 45 of Broca's region; Amunts et al. 1999), aMCC (anterior portion of the midcingulate cortex, encompasses areas a24' and 32'; Vogt et al. 2003; Palomero-Gallagher et al. 2009), anterior insular region (Kurth et al. 2010), CA (cornu ammonis region of the hippocampus; Amunts et al. 2005), Ch1-3 (magnocellular cholinergic cell groups of the basal forebrain; Zaborszky et al. 2008), Fo1 (orbitofrontal area 1; Henssen et al. 2015), Fp2 (frontopolar area Fp2; Bludau et al. 2014), frontal operculum (includes opercular areas op4-op9; Amunts et al. 2010), hIP2 (area 2 on the lateral wall of the intraparietal sulcus; Choi et al. 2006), hIP3 (area 3 on the medial wall of the intraparietal sulcus; Scheperjans, Eickhoff et al. 2008; Scheperjans, Hermann et al. 2008), hOc2 (cytoarchitectonic correlate of the secondary visual cortex; Amunts et al. 2000), ifj2 (area 2 at the inferior frontal junction region; Amunts et al. 2010), IFS (inferior frontal sulcus), LB (laterobasal nucleus of the amygdala; Amunts et al. 2005), MDpr and MDt (parts of the mediodorsal thalamic nucleus connected with the prefrontal and temporal cortices, respectively; Behrens et al. 2003), PFm, PGa and PGp (areas of the inferior parietal lobule; Caspers et al. 2008), pMCC (posterior portion of the midcingulate cortex, encompasses areas p24' and 24d; Vogt et al. 2003; Palomero-Gallagher et al. 2009), premotor (premotor cortex, encompasses the rostral and caudal supplementary motor areas Zilles et al.1996), s24 (subgenual cingulate area s24; Palomero-Gallagher et al. 2008), s32 (subgenual cingulate area s32; Palomero-Gallagher et al. 2008), vPCC (ventral posterior cingulate cortex; encompasses areas v23 and 31; Vogt et al. 2006), WM (white matter). Coordinates are given in anatomical MNI space (Amunts et al. 2005).

and has been involved in sensorimotor gating and motivational behavior (Root et al. 2015), as well as with intraparietal areas hIP2 and hIP3, which, together with the premotor cortex, are part of the sensorimotor network enabling the brain coordination and/or mediation of motor tasks (Ferri et al. 2012). Given the functional connectivity and Behavioural Domain patterns of p24c, one may speculate its role as an integrative hub mediate emotional influences and coordinating motor response, error detection and reorienting processes during events requiring focused attention and sequential information processing.

Functional Fingerprint and Connectivity of p32

Area p32 was associated with a wider range of Behavioural Domains and paradigms than p24ab or p24c. In particular, p32 was significantly activated by higher mental functions such as the theory of mind task, i.e., with cognitive empathy (Walter 2012), and was associated with the specific social cognition Behavioural Domain. The dorsomedial prefrontal cortex constitutes one of the core components of the theory of mind network (Carrington and Bailey 2009; Abu-Akel and Shamay-Tsoory 2011; Schurz et al. 2014; Spunt and Adolphs 2017), and has been subdivided into clusters by means of functional connectivity profiling (Eickhoff, Laird et al. 2016). Area p32 is located at a macroanatomical position on the medial prefrontal cortex comparable to that of the caudal most of these clusters. Furthermore, we also found p32 to be co-activated with the remaining core components of the theory of mind network (Abu-Akel and Shamay-Tsoory 2011; Schurz et al. 2014; Spunt and Adolphs 2017), which are also part of the default mode network (Greicius et al. 2003; Fox, Snyder, et al. 2005; Fransson and Marrelec 2008), i.e., with cytoarchitectonic areas PGa and PGp of the temporo-parietal junction region (Caspers et al. 2006) and with the PCC. In particular the functional connectivity of p32 and areas PGa and PGp is thought to subserve the updating mental representations of the current context and their integration with the appropriate motor response (Geng and Vossel 2013).

Interestingly, p32 was also significantly associated with the emotion Behavioural Domains of fear and anxiety, in accordance with previous meta-analytical studies (Phan et al. 2002; Vytal and Hamann 2010; Kirby and Robinson 2017). A closer look at the Paradigm Classes resulting in this association demonstrated that it was not due to activations occurring during the actual emotional experience, but by emotion induction tasks pertaining to the anxiety, fear, and sadness subdomains of emotion processing. Thus, p32 seems to play a crucial role in the cognitive regulation of emotion, but not in the activations occurring during the actual processing of emotionally valenced stimuli. Area p32 is thought to be a key player in the neural circuit subserving the renewal of extinguished fear memory, whereby it serves node which integrates contextual information from hippocampal inputs, and projects this information to

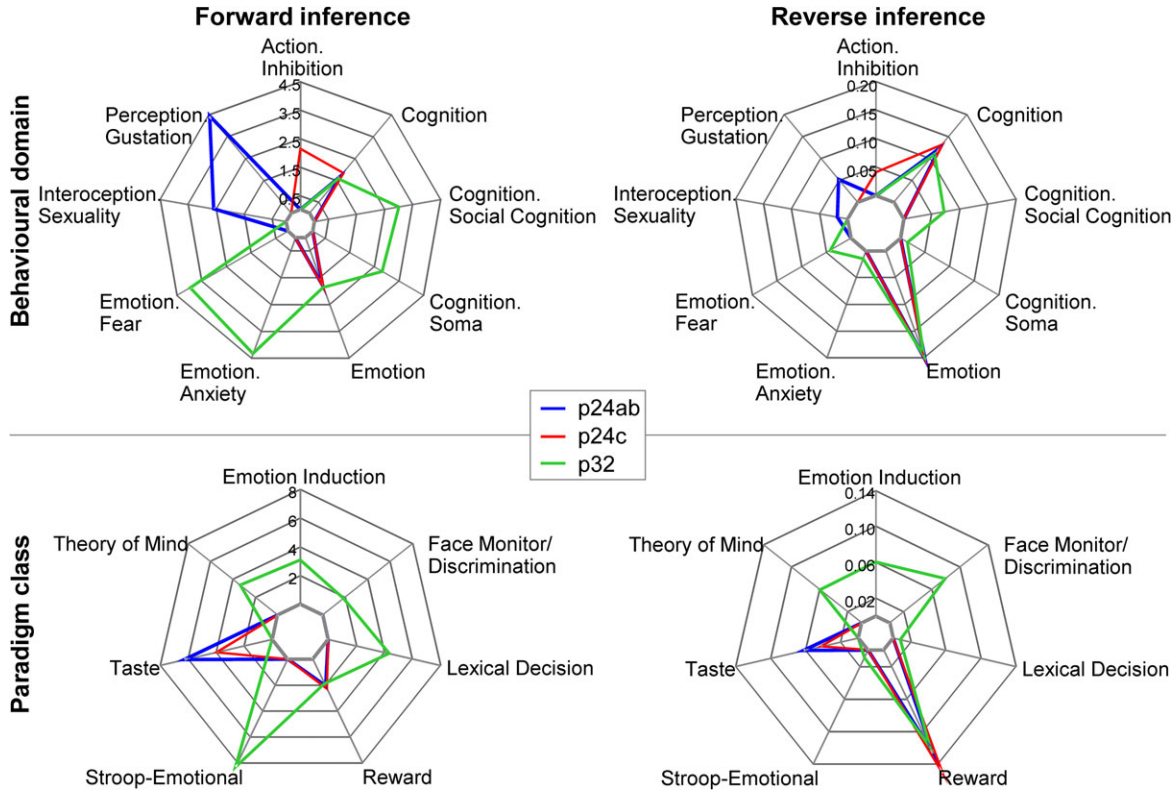

Figure 7. Functional fingerprint of p24ab, p24c, and p32 depicting significant associations with Behavioural Domains (top row; P(Activation|Domain)) and Paradigm Classes (bottom row; P(Domain|Activation)) of the BrainMap meta-data (www.brainmap.org; category labeling in the polar plots). Axis labeling in plots of the left column indicates the likelihood ratio values determined in the forward inference. Axis labeling in plots of the right column indicates the probability values determined in the reverse inference analysis.

the amygdala, thus enabling context-dependent fear responses (Chen et al. 2017). Additionally, our contrast analyses of the functional connectivity pattern of p32 also revealed that it was strongly associated with both the amygdala and the CA1 region of the hippocampus, probably reflecting true anatomical connectivity, as seen in non-human primate and rodent brains. Indeed, in macaque monkeys area 32 receives efferents from the CA1 region (Vogt and Pandya 1987; Insausti and Muñoz 2001; Yukie and Shibata 2009); and is reciprocally connected with the amygdala (Van Hoesen 1981; Amaral and Price 1984; Stefanacci and Amaral 2000; Yukie and Shibata 2009). In rodents the infralimbic cortex—i.e., the putative homolog of human area 32 (Vogt et al. 2013)—is targeted by robust afferents from the CA1 region (Jay and Witter 1991), and projects to the amygdala (Buchanan et al. 1994; Hoover and Vertes 2007). We also found a strong association of p32 with the mediodorsal thalamic nucleus. Specifically, with MDpr and MDt, as defined in the human brain by Behrens et al. (2003) using diffusion imaging data. Association of p32 with MDpr is not surprising given that the mediodorsal nucleus is reciprocally connected with the prefrontal cortex (e.g., Tobias 1975; Tanaka 1976; Vogt et al. 1987). Since diffusion weighted imaging is sensitive only to the orientation of fiber tracts, but not to their polarity, connectivity between the mediodorsal nucleus and the temporal pole is thought (Behrens et al. 2003) to reflect efferents to this part of the thalamus from the amygdala, temporal pole, and inferior temporal areas TE and TEO (Aggleton and Mishkin 1984; Russchen et al. 1987; Webster et al. 1993). Finally, although efferents from area 32 to the posterior orbitofrontal cortex have been described in the monkey brain (Garcia-Cabezas and Barbas 2017), we found no significant co-activation pattern between p32 and orbitofrontal areas. This could be a false negative finding resulting from the frequently described difficulties with echo planar imaging related distortions and signal dropout in the orbitofrontal cortex.

Cytoarchitectonic and Functional Gradations Within ACC

Areas within the ACC present a clear cytoarchitectonic gradation (Sanides 1962) when moving from area 33 either through the subdivisions of area s24 (s24a, s24b) into area s32, or through the subdivisions of area p24 (p24a, p24b, pd24cv, pd24cd) into s32 (Palomero-Gallagher et al. 2008). An additional gradation is seen when moving from area 25 through the areas within sACC into those of pACC (Palomero-Gallagher et al. 2008). Both gradations are characterized by an increasing differentiation of the cortical lamination, and this is particularly true for the changes occurring in the caudal-to-rostral direction. Area 33 presents the most “primitive” cytoarchitectonic organization within the ACC, since no distinct layers can be distinguished (Palomero-Gallagher et al. 2008). Area 33 is followed in the callosal sulcus by periallocortical agranular areas s24 and p24, characterized by a particularly prominent layer V which is easily delineable from layers III and VI due to the large densely packed pyramids as in Va and the cell sparse Vb. Areas s24 and p24 are followed by dysgranular isocortical areas s32 and p32, respectively, each with a considerably less prominent layer V (Palomero-Gallagher et al. 2008). The changes in lamination when moving from areas of the sACC dorsally into areas of the

pACC are more subtle, and mostly restricted to gradation differences in the size of layer III pyramids (Palomero-Gallagher et al. 2008). Whereas in areas of s24 layer III contains clearly larger pyramids near the surface than at the border with layer V, in p24 layer III pyramids only taper down slightly in size when approaching layer V. Likewise, layer IIIc pyramids of area p32 are larger than those of area s32 (Palomero-Gallagher et al. 2008).

These 2 cytoarchitectonic gradation directions (when moving from the callosal sulcus to the convexity of the hemisphere, or when moving from sACC into pACC), and the increasing complexity in the degree of lamination they entail, are paralleled by gradual changes in the cognitive demand associated with the tasks activating the different sACC and pACC areas. All cytoarchitectonic areas of the ACC could be associated with the processing of emotions (present results and Palomero-Gallagher et al. 2015). However, whereas areas of the sACC are activated during the subjective perception of the body state or the actual experiencing of negatively valenced emotions (Palomero-Gallagher et al. 2015), we here found the areas of the pACC to be associated with tasks requiring associative processes requiring an increasing integration of information processing levels. Thus, area p24ab was linked to the phenomenological experience of the body state, which involves the integration of somatic information pertaining all aspects of the body's physiological condition with subjective time perception and emotional memories (Craig 2002; Wiens 2005; Ceunen et al. 2016). Area p24c was specifically associated with the inhibition of action, i.e., the suppression of unwanted reflex-like actions and the control of voluntary movement, which requires the coordination of processes associated with sustained and selective attention, motor timing and withdrawal of a planned response (Faw 2003; Miller and Wallis 2009). Finally, p32 was significantly associated with processes ultimately resulting in the ability to mentalize the emotions of others, i.e., to experience empathy (Walter 2012). Area p32 was activated by emotion induction tasks pertaining negatively valenced stimuli as well as by tasks probing the subject's ability to evaluate, respond to, and provide verbal information about bodily sensations, feelings, thoughts and experiences. More importantly, p32 was also associated with the ability to share another's internal world of thoughts and feelings. Thus, area p32 could be classified as cingulate association cortex playing a crucial role in the cognitive regulation of emotion.

Supplementary Material

Supplementary material is available at *Cerebral Cortex* online.

Funding

This study was partially supported by the European Union's Horizon 2020 Research and Innovation Programme under Grant Agreement No. 785907 (HBP SGA2), the National Institute of Mental Health (R01-MH074457), and the Helmholtz Portfolio Theme "Supercomputing and Modeling for the Human Brain."

Notes

Conflict of interest: The authors have no conflict of interest to declare.

References

Abu-Akel A, Shamay-Tsoory S. 2011. Neuroanatomical and neurochemical bases of theory of mind. Neuropsychologia. 49: 2971–2984.

Aggleton JP, Mishkin M. 1984. Projections of the amygdala to the thalamus in the cynomolgus monkey. J Comp Neurol. 222:56–68.

Allman JM, Hakeem A, Erwin JM, Nimchinsky E, Hof P. 2001. The anterior cingulate cortex. The evolution of an interface between emotion and cognition. Ann NY Acad Sci. 935:107–117.

Amaral DG, Price JL. 1984. Amygdalo-cortical projections in the monkey (Macaca fascicularis). J Comp Neurol. 230:465–496.

Amunts K, Hawrylycz MJ, van Essen DC, Van Horn JD, Harel N, Poline JB, De Martino F, Bjaalie JG, Dehaene-Lambertz G, Dehaene S, et al. 2014. Interoperable atlases of the human brain. Neuroimage. 99:525–532.

Amunts K, Kedo O, Kindler M, Pieperhoff P, Mohlberg H, Shah NJ, Habel U, Schneider F, Zilles K. 2005. Cytoarchitectonic mapping of the human amygdala, hippocampal region and entorhinal cortex: intersubject variability and probability maps. Anat Embryol. 210:343–352.

Amunts K, Lenzen M, Friederici AD, Schleicher A, Morosan P, Palomero-Gallagher N, Zilles K. 2010. Broca's region: novel organizational principles and multiple receptor mapping. PLoS Biol. 8. doi:10.1371/journal.pbio.1000489.

Amunts K, Malikovic A, Mohlberg H, Schormann T, Zilles K. 2000. Brodmann's areas 17 and 18 brought into stereotaxic space-where and how variable? Neuroimage. 11:66–84.

Amunts K, Schleicher A, Bürgel U, Mohlberg H, Uylings HBM, Zilles K. 1999. Broca's region revisited: cytoarchitecture and intersubject variability. J Comp Neurol. 412:319–341.

Aron AR, Robbins TW, Poldrack RA. 2004. Inhibition and the right inferior frontal cortex. Trends Cogn Sci. 8:170–177.

Aron AR, Robbins TW, Poldrack RA. 2014. Inhibition and the right inferior frontal cortex: one decade on. Trends Cogn Sci. 18:177–185.

Beckmann M, Johansen-Berg H, Rushworth MF. 2009. Connectivity-based parcellation of human cingulate cortex and its relation to functional specialization. J Neurosci. 29: 1175–1190.

Behrens TE, Johansen-Berg H, Woolrich MW, Smith SM, Wheeler-Kingshott CA, Boulby PA, Barker GJ, Sillery EL, Sheehan K, Ciccarelli O, et al. 2003. Non-invasive mapping of connections between human thalamus and cortex using diffusion imaging. Nat Neurosci. 6:750–757.

Bludau S, Eickhoff SB, Mohlberg H, Caspers S, Laird AR, Fox PT, Schleicher A, Zilles K, Amunts K. 2014. Cytoarchitecture, probability maps and functions of the human frontal pole. Neuroimage. 93:260–275.

Brodmann K. 1909. Vergleichende Lokalisationslehre der Großhirnrinde in ihren Prinzipien dargestellt auf Grund des Zellbaues. Barth: Leipzig.

Brodmann K. 1910. Feinere Anatomie des Großhirns. In: Lewandowsky M, editor. Handbuch der Neurologie. Erster Band. Allgemeine Neurologie. Berlin: Springer. p. 206–307.

Buchanan SL, Thompson RH, Maxwell BL, Powell DA. 1994. Efferent connections of the medial prefrontal cortex in the rabbit. Exp Brain Res. 100:469–483.

Bush G, Luu P, Posner MI. 2000. Cognitive and emotional influences in anterior cingulate cortex. Trends Cogn Sci. 4:215–222.

Carrington SJ, Bailey AJ. 2009. Are there theory of mind regions in the brain? A review of the neuroimaging literature. Hum Brain Mapp. 30:2313–2335.

Caspers S, Eickhoff SB, Geyer S, Scheperjans F, Mohlberg H, Zilles K, Amunts K. 2008. The human inferior parietal lobule in stereotaxic space. Brain Struct Funct. 212:481–495.

Caspers S, Geyer S, Schleicher A, Mohlberg H, Amunts K, Zilles K. 2006. The human inferior parietal cortex: cytoarchitectonic parcellation and interindividual variability. Neuroimage. 33: 430–448.

Ceunen E, Vlaeyen JW, Van Diest I. 2016. On the origin of interoception. Front Psychol. 7:743.

Chen W, Wang Y, Wang X, Li H. 2017. Neural circuits involved in the renewal of extinguished fear. IUBMB Life. 69: 470–478.

Choi H-J, Amunts K, Mohlberg H, Fink GR, Schleicher A, Zilles K. 2006. Cytoarchitectonic mapping of the anterior ventral bank of the intraparietal sulcus in humans. J Comp Neurol. 495:53–69.

Cieslik EC, Zilles K, Caspers S, Roski C, Kellermann TS, Jakobs O, Langner R, Laird AR, Fox PT, Eickhoff SB. 2013. Is there "one" DLPFC in cognitive action control? Evidence for heterogeneity from co-activation-based parcellation. Cereb Cortex. 23: 2677–2689.

Craig AD. 2002. How do you feel? Interoception: the sense of the physiological condition of the body. Nat Rev Neurosci. 3: 655–666.

Craig AD. 2009. How do you feel–now? The anterior insula and human awareness. Nat Rev Neurosci. 10:59–70.

Eickhoff SB, Bzdok D. 2013. Meta-analyses in basic and clinical neuroscience: state of the art and perspective. In: Ulmer S, Jansen O, editors. fMRI. Basics and clinical applications. 2nd ed. Heidelberg: Springer. p. 77–87.

Eickhoff SB, Bzdok D, Laird AR, Kurth F, Fox PT. 2012. Activation likelihood estimation meta-analysis revisited. Neuroimage. 59:2349–2361.

Eickhoff SB, Constable RT, Yeo BT. 2018. Topographic organization of the cerebral cortex and brain cartography. Neuroimage. 170: 332–347.

Eickhoff SB, Grefkes C. 2011. Approaches for the integrated analysis of structure, function and connectivity of the human brain. Clin EEG Neurosci. 42:107–121.

Eickhoff SB, Heim S, Zilles K, Amunts K. 2006. Testing anatomically specified hypotheses in functional imaging using cytoarchitectonic maps. Neuroimage. 32:570–582.

Eickhoff SB, Jbabdi S, Caspers S, Laird AR, Fox PT, Zilles K, Behrens TE. 2010. Anatomical and functional connectivity of cytoarchitectonic areas within the human parietal operculum. J Neurosci. 30:6409–6421.

Eickhoff SB, Laird AR, Fox PT, Bzdok D, Hensel L. 2016. Functional segregation of the human dorsomedial prefrontal cortex. Cereb Cortex. 26:304–321.

Eickhoff SB, Nichols TE, Laird AR, Hoffstaedter F, Amunts K, Fox PT, Bzdok D, Eickhoff CR. 2016. Behavior, sensitivity, and power of activation likelihood estimation characterized by massive empirical simulation. Neuroimage. 137: 70–85.

Eickhoff SB, Stephan KE, Mohlberg H, Grefkes C, Fink GR, Amunts K, Zilles K. 2005. A new SPM toolbox for combining probabilistic cytoarchitectonic maps and functional imaging data. Neuroimage. 25:1325–1335.

Evans AC, Janke AL, Collins DL, Baillet S. 2012. Brain templates and atlases. Neuroimage. 62:911–922.

Faw B. 2003. Pre-frontal executive committee for perception, working memory, attention, long-term memory, motor control, and thinking: a tutorial review. Conscious Cogn. 12:83–139.

Fellows LK, Farah MJ. 2005. Is anterior cingulate cortex necessary for cognitive control? Brain. 128:788–796.

Ferri F, Frassinetti F, Ardizzi M, Costantini M, Gallese V. 2012. A sensorimotor network for the bodily self. J Cogn Neurosci. 24:1584–1595.

Fillinger C, Yalcin I, Barrot M, Veinante P. 2017. Afferents to anterior cingulate areas 24a and 24b and midcingulate areas 24a' and 24b' in the mouse. Brain Struct Funct. 222: 1509–1532.

Fox PT, Laird AR, Fox SP, Fox PM, Uecker AM, Crank M, Koenig SF, Lancaster JL. 2005. BrainMap taxonomy of experimental design: description and evaluation. Hum Brain Mapp. 25: 185–198.

Fox PT, Lancaster JL. 2002. Opinion: mapping context and content: the BrainMap model. Nat Rev Neurosci. 3:319–321.

Fox PT, Lancaster JL, Laird AR, Eickhoff SB. 2014. Meta-analysis in human neuroimaging: computational modeling of large-scale databases. Annu Rev Neurosci. 37:409–434.

Fox MD, Snyder AZ, Vincent JL, Corbetta M, Van Essen D, Raichle ME. 2005. The human brain is intrinsically organized into dynamic, anticorrelated functional networks. PNAS. 102:9673–9678.

Fransson P, Marrelec G. 2008. The precuneus/posterior cingulate cortex plays a pivotal role in the default mode network: evidence from a partial correlation network analysis. Neuroimage. 42:1178–1184.

Garcia-Cabezas MA, Barbas H. 2017. Anterior cingulate pathways may affect emotions through orbitofrontal cortex. Cereb Cortex. 27:4891–4910.

Geng JJ, Vossel S. 2013. Re-evaluating the role of TPJ in attentional control: contextual updating? Neurosci Biobehav Rev. 37:2608–2620.

George MS, Ketter TA, Parekh PI, Horwitz B, Herscovitch P, Post RM. 1995. Brain activity during transient sadness and happiness in healthy women. Am J Psychiatry. 152:341–351.

Greicius MD, Krasnow B, Reiss AL, Menon V. 2003. Functional connectivity in the resting brain: a network analysis of the default mode hypothesis. PNAS. 100:253–258.

Hampshire A, Sharp DJ. 2015. Contrasting network and modular perspectives on inhibitory control. Trends Cogn Sci. 19: 445–452.

Henn S, Schormann T, Engler K, Zilles K, Witsch K. 1997. Elastische Anpassung in der digitalen Bildverarbeitung auf mehreren Auflösungsstufen mit Hilfe von Mehrgitterverfahren. In: Paulus E, Wahl FM, editors. Mustererkennung. Wien: Springer. p. 392–399.

Henssen A, Zilles K, Palomero-Gallagher N, Schleicher A, Mohlberg H, Gerboga F, Eickhoff SB, Bludau S, Amunts K. 2015. Cytoarchitecture and probability maps of the human medial orbitofrontal cortex. Cortex. 75:87–112.

Hoover WB, Vertes RP. 2007. Anatomical analysis of afferent projections to the medial prefrontal cortex in the rat. Brain Struct Funct. 212:149–179.

Hömke L. 2006. A multigrid method for anisotropic PDE's in elastic im age registration. Numer Linear Algebra Appl. 13: 215–229.

Insausti R, Muñoz M. 2001. Cortical projections of the non-entorhinal hippocampal formation in the cynomolgus monkey (Macaca fascicularis). Eur J Neurosci. 14:435–451.

Jay TM, Witter MP. 1991. Distribution of hippocampal CA1 and subicular efferents in the prefrontal cortex of the rat studied by means of anterograde transport of Phaseolus vulgaris-leucoagglutinin. J Comp Neurol. 313:574–586.

Kirby LAJ, Robinson JL. 2017. Affective mapping: an activation likelihood estimation (ALE) meta-analysis. Brain Cogn. 118: 137–148.

Koliatsos VE, Martin LJ, Walker LC, Richardson RT, DeLong MR, Price DL. 1988. Topographic, non-collateralized basal forebrain projections to amygdala, hippocampus, and anterior cingulate cortex in the rhesus monkey. Brain Res. 463: 133–139.

Kross E, Davidson M, Weber J, Ochsner K. 2009. Coping with emotions past: the neural bases of regulating affect associated with negative autobiographical memories. Biol Psychiatry. 65:361–366.

Kurth F, Zilles K, Fox PT, Laird AR, Eickhoff SB. 2010. A link between the systems: functional differentiation and integration within the human insula revealed by meta-analysis. Brain Struct Funct. 214:519–534.

Lancaster JL, Laird AR, Eickhoff SB, Martinez MJ, Fox PM, Fox PT. 2012. Automated regional behavioral analysis for human brain images. Front Neuroinform. 6:23.

Langner R, Rottschy C, Laird AR, Fox PT, Eickhoff SB. 2014. Meta-analytic connectivity modeling revisited: controlling for activation base rates. Neuroimage. 99:559–570.

Levy BJ, Wagner AD. 2011. Cognitive control and right ventrolateral prefrontal cortex: reflexive reorienting, motor inhibition, and action updating. Ann NY Acad Sci. 1224:40–62.

Li CS, Ide JS, Zhang S, Hu S, Chao HH, Zaborszky L. 2014. Resting state functional connectivity of the basal nucleus of Meynert in humans: in comparison to the ventral striatum and the effects of age. Neuroimage. 97:321–332.

Luders E, Toga AW, Thompson PM. 2014. Why size matters: differences in brain volume account for apparent sex differences in callosal anatomy: the sexual dimorphism of the corpus callosum. Neuroimage. 84:820–824.

Lévesque J, Joanette Y, Mensour B, Beaudoin G, Leroux JM, Bourgouin P, Beauregard M. 2003. Neural correlates of sad feelings in healthy girls. Neuroscience. 121:545–551.

Makris N, Seidman LJ, Valera EM, Biederman J, Monuteaux MC, Kennedy DN, Caviness VS Jr., Bush G, Crum K, Brown AB, et al. 2010. Anterior cingulate volumetric alterations in treatment-naive adults with ADHD: a pilot study. J Atten Disord. 13:407–413.

Merker B. 1983. Silver staining of cell bodies by means of physical development. J Neurosci Methods. 9:235–241.

Miller EK, Wallis JD. 2009. Executive function and higher-order cognition: definition and neural substrates. In: Squire LR, editor. Encyclopedia of neuroscience. Oxford: Academic Press. p. 99–104.

Mohlberg H, Eickhoff SB, Schleicher A, Zilles K, Amunts K 2012. A new processing pipeline and release of cytoarchitectonic probabilistic maps - JuBrain. Proceedings of the 18th Annual Meeting of the Organization for Human Brain Mapping. Abstract # 798 p. 191.

Morecraft RJ, Stilwell-Morecraft KS, Cipolloni PB, Ge J, McNeal DW, Pandya DN. 2012. Cytoarchitecture and cortical connections of the anterior cingulate and adjacent somatomotor fields in the rhesus monkey. Brain Res Bull. 87:457–497.

Mufson EJ, Ginsberg SD, Ikonomovic MD, Dekosky ST. 2003. Human cholinergic basal forebrain: chemoanatomy and neurologic dysfunction. J Chem Neuroanat. 26:233–242.

Palomero-Gallagher N, Eickhoff SB, Hoffstaedter F, Schleicher A, Mohlberg H, Vogt BA, Amunts K, Zilles K. 2015. Functional organization of human subgenual cortical areas: relationship between architectonical segregation and connectional heterogeneity. Neuroimage. 115:177–190.

Palomero-Gallagher N, Mohlberg H, Zilles K, Vogt BA. 2008. Cytology and receptor architecture of human anterior cingulate cortex. J Comp Neurol. 508:906–926.

Palomero-Gallagher N, Vogt BA, Schleicher A, Mayberg HS, Schleicher A, Zilles K. 2009. Receptor architecture of human cingulate cortex: evaluation of the four-region neurobiological model. Hum Brain Mapp. 30:2336–2355.

Paus T. 2001. Primate anterior cingulate cortex: where motor control, drive and cognition interface. Nat Rev Neurosci. 2: 417–424.

Perlaki G, Orsi G, Plozer E, Altbacker A, Darnai G, Nagy SA, Horvath R, Toth A, Doczi T, Kovacs N, et al. 2014. Are there any gender differences in the hippocampus volume after head-size correction? A volumetric and voxel-based morphometric study. Neurosci Lett. 570:119–123.

Petrides M, Tomaiuolo F, Yeterian EH, Pandya DN. 2012. The prefrontal cortex: comparative architectonic organization in the human and the macaque monkey brains. Cortex. 48:46–57.

Phan KL, Wager T, Taylor SF, Liberzon I. 2002. Functional neuroanatomy of emotion: a meta-analysis of emotion activation studies in PET and fMRI. Neuroimage. 16:331–348.

Root DH, Melendez RI, Zaborszky L, Napier TC. 2015. The ventral pallidum: subregion-specific functional anatomy and roles in motivated behaviors. Prog Neurobiol. 130:29–70.

Rottschy C, Caspers S, Roski C, Reetz K, Dogan I, Schulz JB, Zilles K, Laird AR, Fox PT, Eickhoff SB. 2013. Differentiated parietal connectivity of frontal regions for “what” and “where” memory. Brain Struct Funct. 218:1551–1567.

Russchen FT, Amaral DG, Price JL. 1987. The afferent input to the magnocellular division of the mediodorsal thalamic nucleus in the monkey, Macaca fascicularis. J Comp Neurol. 256:175–210.

Salzman CD, Fusi S. 2010. Emotion, cognition, and mental state representation in amygdala and prefrontal cortex. Annu Rev Neurosci. 33:173–202.

Sanides F. 1962. Die Architektonik des menschlichen Stirnhirns. Berlin, Göttingen, Heidelberg: Springer.

Scheperjans F, Eickhoff SB, Homke L, Mohlberg H, Hermann K, Amunts K, Zilles K. 2008. Probabilistic maps, morphometry, and variability of cytoarchitectonic areas in the human superior parietal cortex. Cereb Cortex. 18:2141–2157.

Scheperjans F, Hermann K, Eickhoff SB, Amunts K, Schleicher A, Zilles K. 2008. Observer-independent cytoarchitectonic mapping of the human superior parietal cortex. Cereb Cortex. 18:846–867.

Schleicher A, Palomero-Gallagher N, Morosan P, Eickhoff SB, Kowalski T, de Vos K, Amunts K, Zilles K. 2005. Quantitative architectural analysis: a new approach to cortical mapping. Anat Embryol. 210:373–386.

Schurz M, Radua J, Aichhorn M, Richlan F, Perner J. 2014. Fractionating theory of mind: a meta-analysis of functional brain imaging studies. Neurosci Biobehav Rev. 42:9–34.

Seeley WW, Menon V, Schatzberg AF, Keller J, Glover GH, Kenna H, Reiss AL, Greicius MD. 2007. Dissociable intrinsic connectivity networks for salience processing and executive control. J Neurosci. 27:2349–2356.

Seidman LJ, Valera EM, Makris N, Monuteaux MC, Boriel DL, Kelkar K, Kennedy DN, Caviness VS, Bush G, Aleardi M, et al. 2006. Dorsolateral prefrontal and anterior cingulate cortex volumetric abnormalities in adults with attention-deficit/hyperactivity disorder identified by magnetic resonance imaging. Biol Psychiatry. 60:1071–1080.

Smith R, Fadok RA, Purcell M, Liu S, Stonnington C, Spetzler RF, Baxter LC. 2011. Localizing sadness activation within the

subgenual cingulate in individuals: a novel functional MRI paradigm for detecting individual differences in the neural circuitry underlying depression. Brain Imaging Behav. 5:229–239.
Spunt RP, Adolphs R. 2017. The neuroscience of understanding the emotions of others. Neurosci Lett. http://dx.doi.org/10.1016/j.neulet.2017.06.018
Stefanacci L, Amaral DG. 2000. Topographic organization of cortical inputs to the lateral nucleus of the macaque monkey amygdala: a retrograde tracing study. J Comp Neurol. 421: 52–79.
Sturm VE, Sollberger M, Seeley WW, Rankin KP, Ascher EA, Rosen HJ, Miller BL, Levenson RW. 2013. Role of right pregenual anterior cingulate cortex in self-conscious emotional reactivity. Soc Cogn Affect Neurosci. 8:468–474.
Tanaka D Jr. 1976. Thalamic projections of the dorsomedial prefrontal cortex in the rhesus monkey (Macaca mulatta). Brain Res. 110:21–38.
Tobias TJ. 1975. Afferents to prefrontal cortex from the thalamic mediodorsal nucleus in the rhesus monkey. Brain Res. 83: 191–212.
Torta DM, Cauda F. 2011. Different functions in the cingulate cortex, a meta-analytic connectivity modeling study. Neuroimage. 56:2157–2172.
Torta DM, Costa T, Duca S, Fox PT, Cauda F. 2013. Parcellation of the cingulate cortex at rest and during tasks: a meta-analytic clustering and experimental study. Front Hum Neurosci. 7: 275.
van den Heuvel MP, Sporns O. 2013. Network hubs in the human brain. Trends Cogn Sci. 17:683–696.
Van Hoesen GW. 1981. The differential distrib ution, diversity and sprouting of cortical projections to the amygdala in the rhesus monkey. In: Ben Ari Y, editor. The Amygdaloid Complex. New York: Elsevier. p. 77–90.
Vogt BA, Berger GR, Derbyshire SWG. 2003. Structural and functional dichotomy of human midcingulate cortex. Eur J Neurosci. 18:3134–3144.
Vogt BA, Hof PR, Zilles K, Vogt LJ, Herold C, Palomero-Gallagher N. 2013. Cingulate area 32 homologies in mouse, rat, macaque and human: cytoarchitecture and receptor architecture. J Comp Neurol. 521:4189–4204.
Vogt BA, Nimchinsky EA, Vogt L, Hof PR. 1995. Human cingulate cortex: surface features, flat maps, and cytoarchitecture. J Comp Neurol. 359:490–506.
Vogt BA, Pandya DN. 1987. Cingulate cortex of the rhesus monkey: II. Cortical afferents. J Comp Neurol. 262:271–289.
Vogt BA, Pandya DN, Rosene DL. 1987. Cingulate cortex of the rhesus monkey: I. Cytoarchitecture and thalamic afferents. J Comp Neurol. 262:256–270.
Vogt BA, Vogt L, Laureys S. 2006. Cytology and functionally correlated circuits of human posterior cingulate areas. Neuroimage. 29:452–466.
Vytal K, Hamann S. 2010. Neuroimaging support for discrete neural correlates of basic emotions: a voxel-based meta-analysis. J Cogn Neurosci. 22:2864–2885.
Walter H. 2012. Social cognitive neuroscience of empathy: Concepts, circuits, and genes. Emot Rev. 4:9–17.
Webster MJ, Bachevalier J, Ungerleider LG. 1993. Subcortical connections of inferior temporal areas TE and TEO in macaque monkeys. J Comp Neurol. 335:73–91.
Wiens S. 2005. Interoception in emotional experience. Curr Opin Neurol. 18:442–447.
Yukie M, Shibata H. 2009. Temporocingulate interactions in the monkey. In: Vogt BA, editor. Cingulate Neurobiology and Disease. Oxford: Oxford University Press. p. 145–162.
Zaborszky L, Csordas A, Mosca K, Kim J, Gielow MR, Vadasz C, Nadasdy Z. 2015. Neurons in the basal forebrain project to the cortex in a complex topographic organization that reflects corticocortical connectivity patterns: an experimental study based on retrograde tracing and 3D reconstruction. Cereb Cortex. 25:118–137.
Zaborszky L, Hoemke L, Mohlberg H, Schleicher A, Amunts K, Zilles K. 2008. Stereotaxic probabilistic maps of the magnocellular cell groups in human basal forebrain. Neuroimage. 42:1127–1141.
Zilles K, Schlaug G, Geyer S, Luppino G, Matelli M, Qu M, Schleicher A, Schormann T. 1996. Anatomy and transmitter receptors of the supplementary motor areas in the human and nonhuman primate brain. Adv Neurol. 70:29–43.
Zilles K, Schleicher A, Palomero-Gallagher N, Amunts K. 2002. Quantitative analysis of cyto- and receptorarchitecture of the human brain. In: Toga AW, Mazziotta JC, editors. Brain mapping. The methods. 2nd ed. Amsterdam: Elsevier. p. 573–602.
Öngür D, Ferry AT, Price JL. 2003. Architectonic subdivision of the human orbital and medial prefrontal cortex. J Comp Neurol. 460:425–449.